RESEARCH ARTICLE

The role of the NMD factor UPF3B in olfactory sensory neurons

Kun Tan[1†], Samantha H Jones[1†], Blue B Lake[2], Jennifer N Chousal[1], Eleen Y Shum[1], Lingjuan Zhang[3], Song Chen[2], Abhishek Sohni[1], Shivam Pandya[1], Richard L Gallo[3], Kun Zhang[2], Heidi Cook-Andersen[1,4], Miles F Wilkinson[1,5]*

[1]Department of Obstetrics, Gynecology, and Reproductive Sciences, School of Medicine University of California, San Diego, San Diego, United States; [2]Department of Bioengineering, University of California, San Diego, San Diego, United States; [3]Department of Dermatology, University of California, San Diego, San Diego, United States; [4]Division of Biological Sciences, University of California, San Diego, San Diego, United States; [5]Institute of Genomic Medicine, University of California, San Diego, San Diego, United States

Abstract The UPF3B-dependent branch of the nonsense-mediated RNA decay (NMD) pathway is critical for human cognition. Here, we examined the role of UPF3B in the olfactory system. Single-cell RNA-sequencing (scRNA-seq) analysis demonstrated considerable heterogeneity of olfactory sensory neuron (OSN) cell populations in wild-type (WT) mice, and revealed that UPF3B loss influences specific subsets of these cell populations. UPF3B also regulates the expression of a large cadre of antimicrobial genes in OSNs, and promotes the selection of specific olfactory receptor (*Olfr*) genes for expression in mature OSNs (mOSNs). RNA-seq and Ribotag analyses identified classes of mRNAs expressed and translated at different levels in WT and *Upf3b*-null mOSNs. Integrating multiple computational approaches, UPF3B-dependent NMD target transcripts that are candidates to mediate the functions of NMD in mOSNs were identified in vivo. Together, our data provides a valuable resource for the olfactory field and insights into the roles of NMD in vivo.

***For correspondence:** mfwilkinson@health.ucsd.edu

[†]These authors contributed equally to this work

Competing interests: The authors declare that no competing interests exist.

Funding: See page 22

Received: 17 April 2020
Accepted: 09 August 2020
Published: 10 August 2020

Reviewing editor: Didier YR Stainier, Max Planck Institute for Heart and Lung Research, Germany

Introduction

Nonsense-mediated RNA decay (NMD) is a conserved pathway originally discovered by virtue of its ability to degrade aberrant RNAs harboring premature termination codons (PTCs) and thus protect cells from truncated, potentially toxic, dominant-negative proteins (***Chang et al., 2007***; ***Conti and Izaurralde, 2005***; ***Kurosaki et al., 2019***; ***Lykke-Andersen and Jensen, 2015***; ***Palacios, 2013***). Subsequently, it was discovered that NMD degrades subsets of normal RNAs, with loss or disruption of NMD leading to dysregulation of 5–20% of the normal transcriptome in species spanning the phylogenetic scale (***Chan et al., 2007***; ***He et al., 2003***; ***Mendell et al., 2004***). This discovery raised the possibility that the function of NMD extends beyond quality control. This notion has been supported by scores of subsequent studies showing that NMD factors are critical for many fundamental processes, including development, differentiation, cell proliferation, the integrated stress response, the unfolded protein response, and autophagy (***Chang et al., 2007***; ***Karam et al., 2015***; ***Kurosaki et al., 2019***; ***Nasif et al., 2018***).

NMD is well-studied at the biochemical level, with over 15 proteins known to be involved in this pathway (***Chang et al., 2007***; ***Kurosaki et al., 2019***). Three of these proteins—UPF1, UPF2, and UPF3—are present in all eukaryotes and considered to be the core NMD factors (***Conti and Izaurralde, 2005***). UPF1 is an RNA helicase that forms a complex with the adaptor proteins UPF2 and UPF3. In vertebrates, UPF3 is encoded by two paralogs: *UPF3A* (also called '*UPF3*') and *UPF3B* (also

called '*UPF3X*'). UPF3A serves as a weak NMD factor and NMD repressor, while UPF3B is a NMD branch-specific factor that stimulates NMD (**Chan et al., 2007**; **Shum et al., 2016**). UPF3B directly binds to the exon-junction complex (EJC), a large multi-subunit complex recruited to RNAs just upstream of exon-exon junctions after RNA splicing (**Woodward et al., 2017**). The EJC triggers NMD when allowed to interact with other NMD factors. Evidence suggests that EJCs are displaced by the ribosome during the pioneer round of translation, and thus only EJCs deposited downstream of the stop codon defining the main open-reading frame (ORF) are able to elicit NMD (**Dostie and Dreyfuss, 2002**). Ribosomes would also be predicted to displace the last EJC when the termination codon resides ~50 nucleotides or less upstream of the last exon-exon junction, based on the length of the EJC and ribosome footprints. This has led to the '−50-nt boundary rule,' an empirically verified dictum which states that only in-frame stop codons further than ~50 nt upstream of the last exon-exon junction elicit NMD (**Nagy and Maquat, 1998**). While there are exceptions to this −50-nt boundary rule (**Carter et al., 1996**), it reliably predicts a large proportion of EJC-dependent NMD target mRNAs (**Boehm et al., 2014**; **Gehring et al., 2005**; **Hurt et al., 2013**). NMD can be triggered by other molecular signals in addition to downstream EJCs. For example, long 3'-untranslated regions (UTRs) and short ORFs upstream of the main ORF (uORFs) can, in some cases, trigger NMD in an EJC-independent manner (**Barrett et al., 2012**; **Bühler et al., 2006**; **Chang et al., 2007**; **Hurt et al., 2013**; **Kebaara and Atkin, 2009**; **Rebbapragada and Lykke-Andersen, 2009**).

While considerable progress has been made in understanding the molecular features that elicit NMD, we are still largely in the dark with regard to which transcripts are targeted for rapid decay. It is critical to define such NMD target mRNAs in order to begin to unravel the molecular mechanisms by which NMD influences biological processes. A particularly large gap in the field is the identity of NMD targets in vivo.

Many lines of evidence suggests that NMD is not a single linear pathway but instead consists of several branches, each of which depends on different factors and promotes the decay of different sets of transcripts (**Chan et al., 2007**; **Gehring et al., 2005**; **Mabin et al., 2018**). In this report, we focus on the UPF3B-dependent branch of NMD, which has been shown to be important for the nervous system. Pedigree analysis of numerous families harboring mutations in the *UPF3B* gene have demonstrated that both nonsense and missense mutations cause intellectual disability in humans (**Nguyen et al., 2014**; **Tarpey et al., 2007**). Humans with *UPF3B* mutations also commonly have autism, schizophrenia, and/or attention-deficit/hyperactivity disorder (**Nguyen et al., 2014**; **Tarpey et al., 2007**). To understand the underlying mechanism for these behavioral defects, we generated *Upf3b*-deficient mice (**Huang et al., 2011**; **Karam et al., 2015**). These *Upf3b*-null mice suffer from specific learning and memory deficits, including fear-conditioned learning, and thus replicate some aspects of the behavioral defects in UPF3B-deficient humans (**Huang et al., 2018**). In part, these behavioral defects may stem from abnormal neural connectivity, as cortical pyramidal neurons from *Upf3b*-null mice undergo impaired dendritic spine maturation in vivo (**Huang et al., 2018**). Furthermore, cultured UPF3B-depleted neural cells have subtle dendrite outgrowth defects (**Jolly et al., 2013**), and expression of UPF3B mutants reduces neurite branching (**Alrahbeni et al., 2015**). The behavioral defects in *Upf3b*-null mice may also result from neural differentiation and/or maturation defects that were uncovered using loss-of-function approaches in neural precursor cells in vitro, or by forced expression of UPF3B mutants in cell lines in vitro (**Alrahbeni et al., 2015**; **Huang et al., 2018**; **Jolly et al., 2013**).

In this communication, we examine the role of UPF3B in the olfactory system, a useful model for studying neural development and function. There is also considerable clinical interest in the olfactory system, as olfactory defects predict the later onset of numerous CNS disorders, including Parkinson's and Alzheimer's disease (**Doty, 2012**). Olfactory dysfunction also strongly associates with autism (**Rozenkrantz et al., 2015**). The olfactory epithelium (OE) retains a life-long capacity for neurogenesis and harbors a robust regeneration system that responds to injury (**Whitman and Greer, 2009**). Importantly, the olfactory system is much simpler than the CNS. Mature olfactory sensory neurons (mOSNs) develop via a relatively simple linear pathway involving horizontal basal cells (HBCs), globose basal cells (GBCs), and immature olfactory sensory neurons (iOSNs). Both HBCs and GBCs are stem cells, but the two types have different roles (**Schwob et al., 2017**). HBCs are reserve stem cells, as they are normally quiescent and only undergo proliferative expansion in response to OE injury (**Peterson et al., 2019**). In contrast, GBCs are a heterogeneous cell population that consists of constitutively active stem cells as well as progenitors (**Schwob et al., 2017**). Lineage-tracing analysis

and single-cell RNA sequencing (scRNA-seq) analysis have shown that after proliferative expansion, HBCs and GBCs give rise to iOSNs, which are responsible for undergoing maturation (**Fletcher et al., 2017**). Of note, iOSNs share markers with another OSN stage called 'immediate neural precursors (INPs)." Given the ambiguity of the nomenclature, we will refer to cells with either INP or iOSN characteristics as iOSNs. iOSNs ultimately differentiate into mOSNs, which send an axon to neurons in the glomeruli region of the olfactory bulb, relaying olfactory information from the outside world to the CNS. mOSNs recognize odorants through chemosensory receptors, including olfactory receptors (OLFRs), members of the G-protein-coupled receptor super-family, as well as trace amine–associated receptors, guanylate cyclases, and members of the membrane-spanning 4-pass A gene family (**Bear et al., 2016**; **Saraiva et al., 2019**).

To gain insight into the nature of the cells in the OE and their developmental relationships, recent studies have performed transcriptome profiling using whole OE, pools of sorted OSNs, single OSNs, or single OE cells (**Fletcher et al., 2017**; **Ibarra-Soria et al., 2014**; **Saraiva et al., 2015**; **Saraiva et al., 2019**; **Tan et al., 2015**). These studies have revealed new OE cell subsets, inferred the developmental pathways of both OSN and non-neural OE cells, defined classes of genes exhibiting enriched expression and unique patterns of expression in different OE subsets, and revealed the expression patterns and dynamics of OLFRs during OSN development and in individual mOSNs. These studies have also advanced our understanding of mammalian olfaction evolution.

In this study, we ascertain whether the NMD factor, UPF3B, has roles in the olfactory system. Using scRNA-seq and RNA-seq analyses, we obtained evidence that UPF3B influences the frequency of specific OSN subsets, broadly suppresses the expression of immune genes in OSNs, and shapes the *Olfr* gene repertoire. We also identified high-confidence NMD target mRNAs in vivo that are candidates to act downstream of UPF3B in mOSNs. As part of our analysis, we also provide new cellular and molecular information on WT OSNs and their development in vivo. Our findings in *Upf3b*-null NMD-deficient mice introduce a useful biological system to understand the role of RNA metabolism in neurons, and our scRNA-seq, RNA-seq, and RiboTag datasets are new resources that can be used by the olfactory field.

Results

UPF3B-regulated genes in mOSNs

To assess whether NMD-deficient *Upf3b*-null mice have an olfactory defect, we measured their weight during their growth phase. This follows from the fact that newborn mice are blind and therefore depend on the olfactory system to initiate milk suckling for survival (**Logan et al., 2012**). We quantified the weight of *Upf3b*-null and littermate WT mice and found that *Upf3b*-null mice have a statistically significant postnatal weight deficit ($p<0.05$; **Figure 1A**). The weight deficit occurs soon after birth, becomes progressively worse during postnatal development, and is corrected after reaching adulthood. This specific pattern of weight loss is characteristic of mice harboring a partial olfactory defect (**Riera et al., 2017**). In contrast, newborn mice that completely lack sense of smell are incapable of sensing their source of milk and die soon after birth (**Hongo et al., 2000**). As further evidence that *Upf3b*-null mice have an olfactory defect, we found that HBC, iOSN and mOSN marker genes (*Krt5, Gap43*, and *Gnal*, respectively) exhibited significantly decreased expression in *Upf3b*-null as compared to WT OE (**Figure 1B**). We followed up by testing *Upf3b*-null mice for evidence for specific olfactory deficits and observed trends but did not observe statistically significant effects (**Figure 1—figure supplement 1A**), providing further evidence of a partial olfactory defect.

Given that mOSNs are the functional units of the OE, we next focused our attention on these cells. We identified UPF3B-regulated genes in mOSNs by performing RNA-seq analysis on FACS-purified mOSNs (YFP+ cells) from R26-eYFP; *Omp*-Cre mice (**Figure 1—figure supplement 1B**). Four samples were analyzed from each genotype (**Figure 1—figure supplement 2A** and **Supplementary file 1**). The expression of OSN precursor/OSN canonical markers are shown in **Figure 1—figure supplement 2D**. RNA-seq analysis identified 235 differentially expressed genes between *Upf3b*-null and WT mOSNs ($q < 0.05$) (**Figure 1C** and **Supplementary file 2**). We validated our RNA-seq analysis by qPCR analysis and immunofluorescence (**Figure 1—figure supplement 2B, C**).

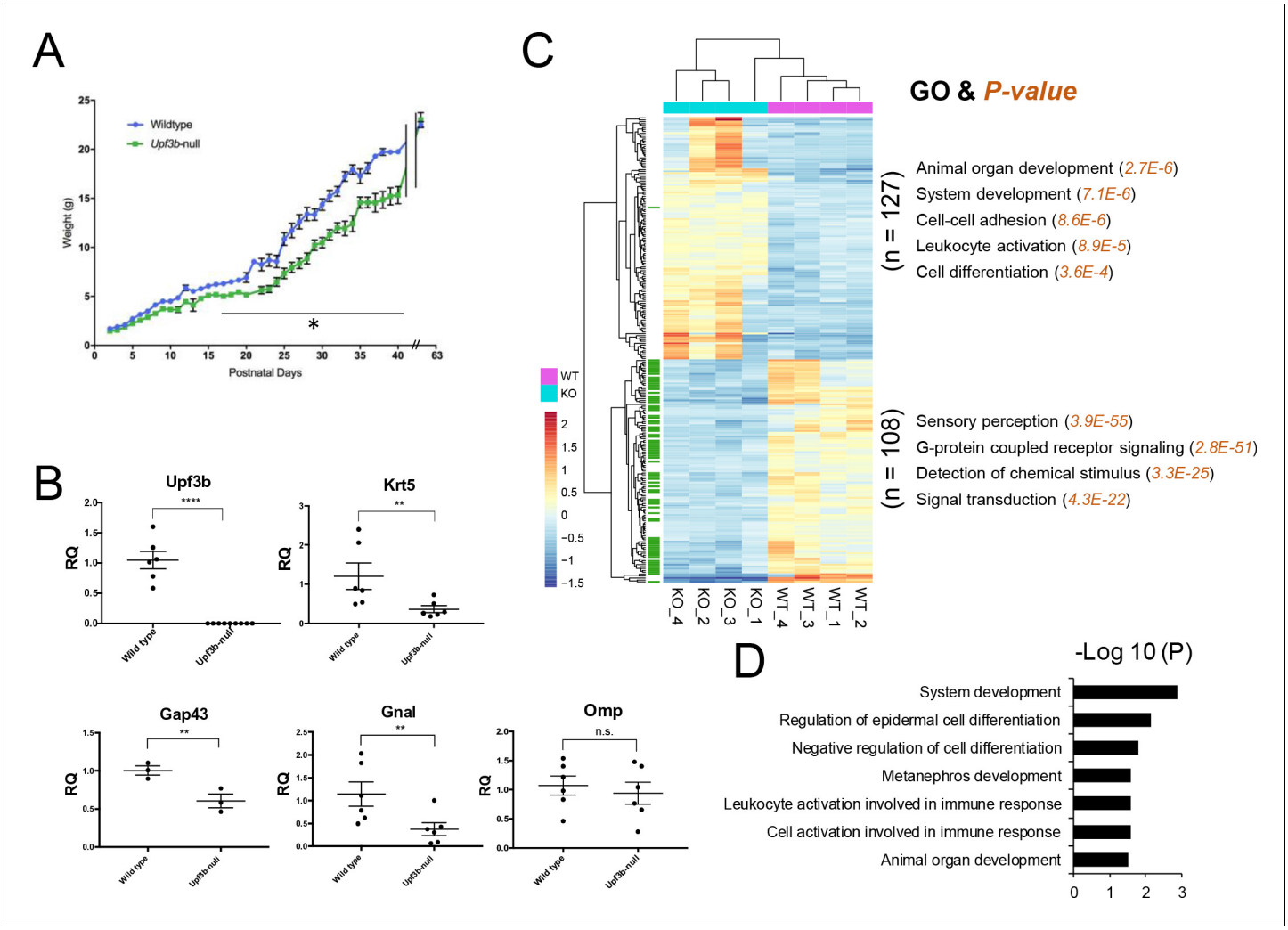

Figure 1. Identification of UPF3B-regulated genes and NMD target genes in the olfactory system. (**A**) The weight of *Upf3b*-null vs. WT (wild type) mice at the indicated time points. *Upf3b*-null mice gain weight slowly during postnatal development but then reach the weight of WT mice at the last time point (9 weeks), a pattern indicative of a partial olfactory defect. *, p<0.05. (**B**) qPCR analysis of olfactory marker genes in *Upf3b*-null and WT OE (n = 6). **, p<0.01; ****, p<0.0001. (**C**) Heatmap of genes differentially expressed in mOSNs from *Upf3b*-null (KO) vs. WT mice (four biological replicates from each are shown). Row names labeled as green are *Olfr* genes. Right, the most statistically significant GO terms associated with upregulated genes (top) and downregulated genes (bottom) after *Upf3b* loss. (**D**) A list of most statistically enriched GO terms associated with the 52 high-confidence UPF3B-dependent NMD target mRNAs we identified in mOSNs.

The online version of this article includes the following figure supplement(s) for figure 1:

Figure supplement 1. Upf3b-null mice behavior and purified mOSNs.

Figure supplement 2. UPF3B-regulated genes in mOSNs.

Among the 127 upregulated genes were several involved in neurogenesis, including *Lrp2*, *Hk2*, *Notch2*, *Gdf11*, *Fos*, *Ptch1*, and *Spry2*. Gene ontology (GO) analysis revealed enrichment for 'organ/system development,' 'cell-cell adhesion,' 'leukocyte activation,' and 'cell differentiation/proliferation' functions (***Figure 1C***). In contrast, the 108 downregulated genes were most enriched for GO functions associated with olfaction: 'sensory perception,' 'G-proteins,' 'detection of chemical stimulus,' and 'signal transduction.' Indeed, we found that the majority (78 out of 108) of these significantly downregulated genes are *Olfr* genes (marked in green in ***Figure 1C***; the expression of all *Olfr* genes in *Upf3b*-null and control mOSNs is shown in ***Figure 1—figure supplement 2E*** and ***Supplementary file 1***). We follow-up on this surprising finding below. Other genes downregulated in *Upf3b*-null mOSNs include those involved in CNS synaptic transmission (*Slc17a6*), chromatin remodeling (*Chd1*), and sensory neuronal plasticity (*Cwc22*) (***Supplementary file 2***).

Identification of NMD target mRNAs in mOSNs

NMD is thought to influence biological systems by virtue of its ability to promote the decay of specific subsets of mRNAs (***Lykke-Andersen and Jensen, 2015***). As described in the introduction, there is dearth of knowledge regarding the identity of such NMD target RNAs, particularly in cells in their normal in vivo context. Our RNA-seq analysis of purified mOSNs from *Upf3b*-null and WT mice provided an opportunity to identify in vivo direct NMD targets. Because NMD is a negative regulatory pathway (it degrades its targets), the 127 RNAs *upregulated* in *Upf3b*-null mOSNs are candidates to be direct NMD targets. Among them, we found that 73 had at least one of the well-established molecular features known to elicit NMD, including an exon-exon junction >50 nt downstream of the main ORF (dEJ) (***Table 1***; see the Introduction for an explanation of NMD-inducing features [NIFs]). Thus, these 73 mRNAs are strong candidates to be UPF3B-dependent NMD target mRNAs in mOSNs.

Given that NMD degrades its target RNAs, this predicts that its targets should be stabilized after inactivation of UPF3B. Thus, we measured the stability of the 127 mRNAs upregulated in *Upf3b*-null mOSNs using a method that infers RNA stability based on pre-mRNA and steady-state mRNA levels (***Alkallas et al., 2017***). This method revealed that 82 of 127 upregulated genes encode mRNAs stabilized in *Upf3b*-null mOSNs as compared to WT mOSNs (***Supplementary file 2***). Of these 82 stabilized and upregulated mRNAs, 52 have at least 1 of the 3 well-established NIFs (***Table 1***), and thus we classified these 52 mRNAs as high-confidence mOSN NMD targets. The statistically enriched GO biological functions of the proteins encoded by these 52 mRNAs are listed in ***Figure 1D***.

Table 1. UPF3B-dependent NMD target mRNAs in mOSNs.

Symbol	log2FC (KO/WT)	Padj	dEJ	uORF	3'UTR length	Symbol	log2FC (KO/WT)	Padj	dEJ	uORF	3'UTR length
Prelid3a	1.099967	0.003745	YES	NO	1572	Fmo2	2.02039	0.014815	NO	NO	2411
1700025G04Rik	0.662926	0.012989	NO	YES	8870	Gab2	0.98414	0.003018	NO	NO	3927
6030419C18Rik	0.73232	0.036112	NO	YES	55	Gdf11	1.429234	0.005353	NO	NO	2811
9330159F19Rik	0.542375	0.017617	NO	YES	3408	Gldn	2.115908	0.045841	NO	NO	2970
Adcy6	2.587005	0.002078	NO	YES	2356	Hk2	2.296045	0.033161	NO	NO	2285
Cdh24	1.560901	0.001303	NO	YES	121	Lbh	1.417311	0.024315	NO	NO	2498
Fam84b	0.719841	0.001704	NO	YES	3969	Luc7l	0.492061	8.19E-05	NO	NO	3738
Inpp5f	1.178064	0.043839	NO	YES	949	Map3k9	0.79841	0.021555	NO	NO	1029
Lrp2	2.504276	0.008534	NO	YES	1305	Msrb3	1.668851	0.033388	NO	NO	2972
Mafg	0.577538	0.046713	NO	YES	4167	Neurl3	1.966306	0.00546	NO	NO	1763
Plxnc1	2.322167	0.048567	NO	YES	2320	Notch2	1.68375	0.047733	NO	NO	2917
Prdm4	0.420203	0.027945	NO	YES	1160	Plekha5	0.608634	0.004216	NO	NO	3461
Ptch1	0.768864	0.01088	NO	YES	3205	Rab43	1.033148	0.0151	NO	NO	3737
Ptger2	3.032221	0.035664	NO	YES	1825	Rac2	3.029035	0.038392	NO	NO	2319
Sash3	2.352656	0.033245	NO	YES	1309	Raver2	1.921185	0.027779	NO	NO	1892
Serpinb11	1.991555	0.002719	NO	YES	468	Rflnb	0.755198	0.017617	NO	NO	2716
Snx33	1.512032	0.012417	NO	YES	1258	Sik1	2.027635	1.48E-06	NO	NO	2035
Zfp36	1.802697	0.025165	NO	YES	774	Slc38a6	1.21151	0.025847	NO	NO	1512
Agap2	1.264604	0.00099	NO	NO	1357	Slc5a1	2.563582	0.00527	NO	NO	1868
Aox2	1.36834	0.018035	NO	NO	1640	Swap70	1.863436	0.009993	NO	NO	2169
Atp10d	3.315656	0.017617	NO	NO	2384	Tgm2	2.395934	0.042993	NO	NO	1399
Bhlhe40	1.435423	0.000192	NO	NO	1593	Themis2	3.496025	0.015464	NO	NO	1053
Btg2	1.281148	0.000173	NO	NO	2199	Tmprss2	2.167673	0.005867	NO	NO	1456
Cybrd1	2.372842	0.002733	NO	NO	4269	Tob2	0.667082	0.001453	NO	NO	2459
Cyth4	2.162221	0.045105	NO	NO	1455	Ywhag	0.644673	0.017707	NO	NO	2586
Ermn	1.686519	0.005793	NO	NO	2641	Zcchc6	0.512078	0.003018	NO	NO	1346

To determine whether these high-confidence NMD target mRNAs correspond to known NMD targets, we assembled a list of likely mouse NMD substrates defined by previous studies (**Supplementary file 3**). To qualify to be in this list, the RNA must have at least one known NMD-inducing feature (NIF) (**Palacios, 2013**) and experimental evidence from at least one assay that it is an NMD substrate (e.g. high UPF1 occupancy or upregulation and/or stabilization in response to NMD-factor depletion). We found that 11 of these previously defined likely mouse NMD target mRNAs overlapped with the 52 high-confidence targets identified in our study: *Atp10d, Lbh, Slc38a6, Tgm2, Notch2, Ywhag, Luc7l, Ptch1, 1700025G04Rik, Ptger2,* and *Msrb3*. Of note, it is not surprising that only a proportion of the upregulated mRNAs we identified in NMD-deficient mOSNs are previously known NMD targets, as NMD target mRNAs can be tissue-, cell type-, and NMD factor-specific (**Huang et al., 2011**). The list of previously defined candidate NMD targets that we compared with were defined in non-neuronal tissues and cell lines made deficient in NMD by knocking down or eliminating factors other than UPF3B (**Supplementary file 3**).

The mOSN transcriptome and translome

We next determined the translation rate of mRNAs in mOSNs, both as a resource for the field and to address the relationship of NMD with translation in vivo. We assayed the translation rate of mRNAs in mOSNs using RiboTag mice, which express an epitope-tagged ribosomal protein, $RPL22^{HA}$, which is incorporated into actively translating ribosomes specifically in cells expressing CRE (**Sanz et al., 2009**). Immunoprecipitation (IP) of the cell lysates of interest with an HA antibody purifies the ribosome-associated mRNAs (**Figure 2A**, left) with an efficiency associated with polysome density (**Hornstein et al., 2016**). To examine ribosome density specifically in WT mOSNs, we isolated RiboTag-labeled mRNA from the OE of *RiboTag; Omp*-Cre mice and performed RNA-seq analysis. As a validation of cell-type specificity, we found that IP of OE lysates with the HA antisera enriched for the mOSN marker, *Omp*, whereas these lysates were depleted of the HBC and GBC markers, *Krt5* and *Lgr5*, respectively (**Figure 2A**, right). We then elucidated inferred translation efficiency (TE) for all expressed mRNAs in mOSNs – the 'mOSN translome' – by calculating the ratio of the IP signal from the RiboTag mice OE lysates over mOSN steady-state mRNA level, the latter determined as described above (**Supplementary file 2**).

Given that 3'UTR length has been shown to influence translation rates in cultured cells (**Spies et al., 2013**), we examined the relationship of 3'UTR length and TE in mOSNs in vivo. We found that mOSN mRNAs harboring 3'UTRs of >2 kb have much higher average TE than mOSN mRNAs harboring shorter 3'UTRs (**Figure 2B**). Highly translated mOSN mRNAs have an average 3'UTR length of ~1.8 kb, while lowly translated mOSN mRNAs have an average 3'UTR length of only ~0.9 kb (**Figure 2C**).

To assess the potential functional relevance of translation, we binned WT mOSN mRNAs into three groups: high (top 30%), medium (middle 40%), and low (bottom 30%) (**Supplementary file 2**). We also binned WT mOSN mRNAs into three groups based on their steady-state level (**Supplementary file 2**), allowing us to place mOSN mRNAs into the nine categories shown in **Figure 2D**. GO analysis revealed that category #1—which is mRNAs expressed at high level that are also highly translated—encode proteins that tend to function in 'metabolism,' 'intercellular transport,' and 'catabolism' (**Figure 2E**). Categories #2 and #3—which are also highly translated mRNAs but less well expressed at the RNA level than category #1—encode proteins with strikingly different functions: 'development,' 'cell migration,' and 'morphogenesis' (**Figure 2E**). Category #6—which is lowly expressed and modestly translated mRNAs—encode proteins involved in 'signal transduction,' 'differentiation,' and 'development,' including 'nervous system development' (**Figure 2E**). The categories with most *Olfr* genes—#4 and #5—are also only moderately translated (**Figure 2E**). *Upf3b*-null mOSNs had similar numbers of mRNAs in the nine categories as WT mOSNs (compare **Figure 2J** with **Figure 2D**), indicative of UPF3B not altering the mOSN transcriptome and translome globally. Rather, UPF3B influences specific mRNAs, as described above for the mOSN transcriptome, and below for the mOSN translome.

The relationship between NMD and translation in vivo

NMD is a translation-dependent pathway, based on protein-synthesis inhibitor and transfection experiments in immortalized cell lines (**Belgrader et al., 1993**; **Carter et al., 1995**; **Karousis and**

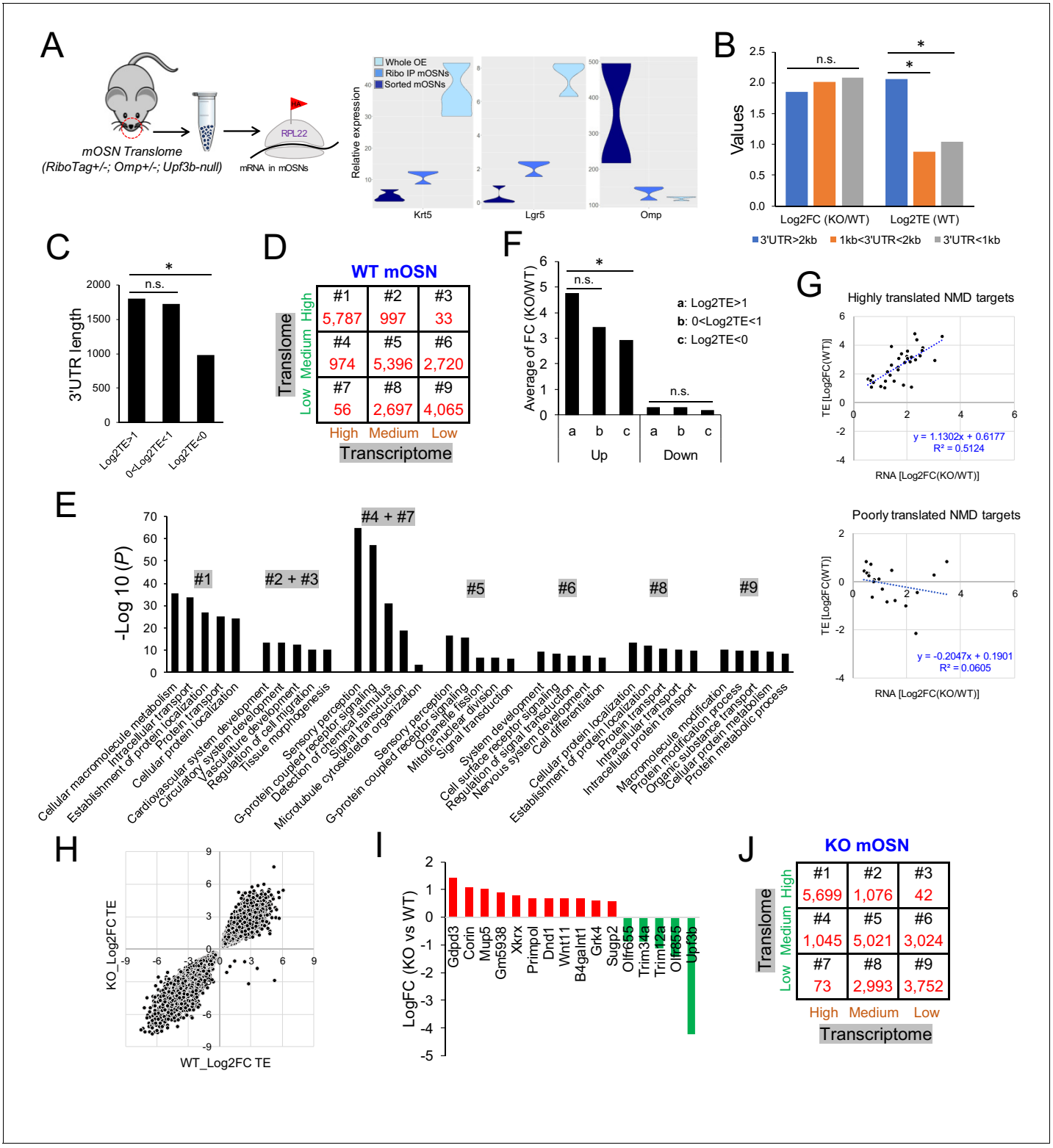

Figure 2. The mOSN translome and NMD. (**A**) Left, strategy used to define the mOSN translome. Right, RNAseq analysis of the expression of gene markers for HBCs (*Krt5*), GBCs (*Lgr5*), and mOSNs (*Omp*) in the indicated samples. (**B**) Average inferred translation efficiency (TE) of mOSN mRNAs with the indicated 3'UTR length ranges. *, p<0.05. (**C**) Average 3'UTR length of mOSN mRNAs with the indicated range of TE values. *, p<0.05. (**D**) mOSN mRNAs from WT mice stratified by steady-state mRNA level (transcriptome) and TE. The number of genes in each category is indicated. (**E**) Top enriched GO terms associated with the different categories of genes defined in (**D**). (**F**) Analysis of upregulated mRNAs (candidate NMD targets) and downregulated mRNAs (indirect targets) are shown on the left and right, respectively. The average shift in expression in *Upf3b*-null mOSNs relative to

Figure 2 continued on next page

Figure 2 continued

WT mOSNs is shown for mOSNs binned by TE (a and c have the highest and lowest TE values, respectively). *, p<0.05. (**G**) Scatter plot of the 52 high-confidence mOSN NMD targets, showing TE vs. NMD magnitude (upregulation in *Upf3b*-null mOSNs). Both values are log2-transformed. (**H**) Scatterplot showing the TE of mRNAs in *Upf3b*-null vs. WT mOSNs. (**I**) mRNAs exhibiting significantly altered TE in response to *Upf3b* loss. (**J**) mOSN mRNAs from *Upf3b*-null (KO) mice stratified by steady-state mRNA level (transcriptome) and TE. The number of cells in each category is indicated.

Mühlemann, 2019). Our mOSN transcriptome and translome data from *Upf3b*-null and WT mice provided an opportunity to address the relationship of NMD with translation in vivo. Given that higher translation rates allow for a higher frequency of stop codon recognition, it follows that higher translation rates might drive stronger NMD. This predicts that more highly translated mOSN mRNAs will have a higher NMD response than lowly translated mOSN mRNAs. To test this, we binned mRNAs statistically upregulated in *Upf3b*-null mOSNs into three groups stratified by TE. The most highly translated group was statistically more upregulated (i.e., had stronger NMD) than the least translated group (***Figure 2F***, left). As a negative control, we examined downregulated mRNAs (as these would not be direct NMD targets) and found no statistical difference between degree of downregulation and TE (***Figure 2F***, right).

To further examine whether high translation rate is associated with strong NMD magnitude, we binned the 52 high-confidence NMD substrates we defined above into two groups: those with little or no translation and those with high translation (cut-off: log2TE > 1). We then independently plotted these two sets of mRNAs in terms of TE and NMD magnitude (i.e. the degree of upregulation in *Upf3b*-null mOSNs relative to WT mOSNs). The results show that the high-translation group exhibited a correlation between their inferred translation rate and NMD magnitude (R^2 = 0.5; ***Figure 2G***). In contrast, the low-translation group of mRNAs exhibited no correlation between their translation rate and NMD magnitude (R^2 = 0.06; ***Figure 2G***). Together, these results support that NMD is translation-dependent in vivo and that its magnitude tends to be enhanced for highly translated mRNAs.

Our mOSN translome data also allowed us to assess the reciprocal question: does *Upf3b* influence translation in vivo? When we plotted the TE of mRNAs when expressed in *Upf3b*-null mOSNs vs. when expressed in WT mOSNs, we found that the vast majority of mRNAs were similarly translated in both genetic backgrounds, as measured by RiboTag analysis (***Figure 2H***, ***Supplementary file 2***). Only 16 mOSN mRNAs migrated off the diagonal and thus had a significant change in TE as a result of *Upf3b* loss (***Figure 2H,I***).

Identification of OE cell clusters

To determine whether UPF3B influences the cellular composition of the OE, we performed scRNA-seq analysis on dissociated OE cells from 4 *Upf3b*-null and 4 WT mice. After filtering out poor quality cells, 25,165 cells remained for subsequent analysis. Biological replicates exhibited similar cell distributions (***Figure 3A***). Using a nonlinear dimensionality-reduction technique—uniform manifold approximation and projection (UMAP)—we identified cell clusters corresponding to 16 known cell types in the OE (***Figure 3B***). Some of the gene markers used to define these cell clusters are shown in ***Figure 3C***. Genes exhibiting enriched expression in each of the 16 cell types are listed in ***Supplementary file 4***.

Re-clustering of OSN precursors/OSNs (HBCs, GBCs, iOSNs, and mOSNs) revealed several cell sub-clusters within each of these four stages (***Figure 3D,E***). The identification of these sub-clusters suggested that each of these developmental stages exhibit considerable heterogeneity, at least at the transcriptome level. Genes exhibiting enriched expression in each sub-cluster are shown in ***Supplementary file 4***.

HBC are known to be reserve stem cells, while GBCs consist of active stem cells and progenitors (***Schwob et al., 2017***). Consistent with this, cell-cycle analysis showed that all four HBC sub-clusters primarily contain quiescent cells, while the GBC sub-clusters have many cells that are proliferating (***Figure 3F***). All four HBC sub-clusters express similar levels of well-established HBC markers, including *Krt5* and *Trp63* (***Figure 4A***). These HBC sub-clusters are each uniquely marked by novel gene markers that we identified (***Figure 4A*** and ***Supplementary file 4***).

GBCs also segregated into four sub-clusters (***Figure 3D***), which is consistent with past studies demonstrating that GBCs are heterogeneous (***Cau et al., 1997***; ***Manglapus et al., 2004***; ***Schwob et al., 2017***). Monocle pseudotime trajectory analysis suggested that these four sub-

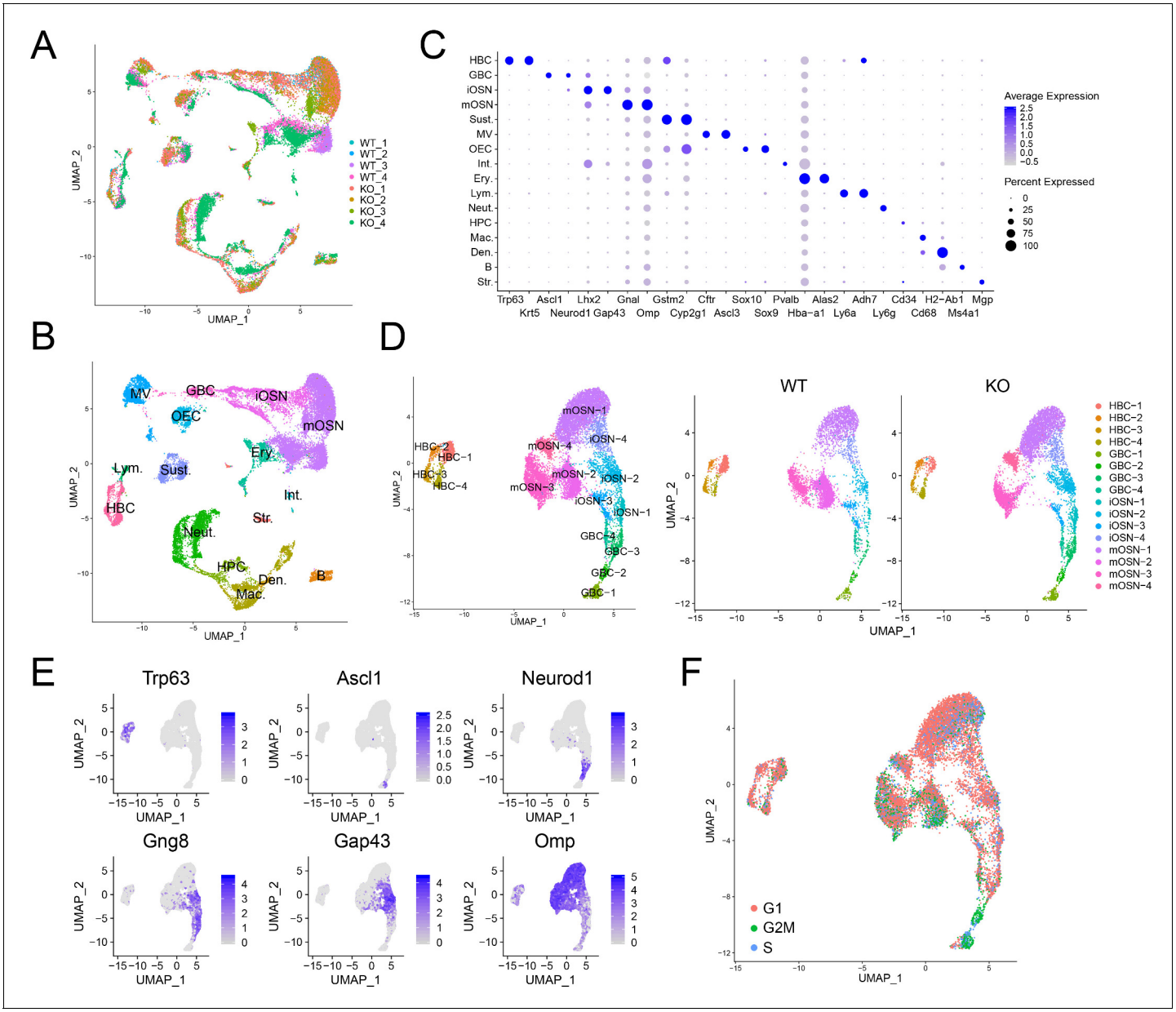

Figure 3. Identification of OE cell subsets using scRNAseq analysis. (**A**) UMAP plot of OE cells from 4 *Upf3b*-null (KO) and 4 WT mice analyzed by scRNAseq. (**B**) Same UMAP plot as is in (**A**), showing the identity of the different cell clusters. (**C**) Dotplot depicting the expression of gene markers in the cell clusters defined in (**B**). (**D**) Left, UMAP plot of reclustered OSN precursors/OSNs defined in (**A**). Right, genotype information. (**E**) Same UMAP plot as in (**D**), showing the expression of stage-specific markers. (**F**) Same UMAP plot as in (**D**), showing inferred cell-cycle phase based on the expression of a large set of G2/M- and S-phase genes (***Kowalczyk et al., 2015***).

clusters have a linear developmental relationship, with GBC-1 the most immature, GBC-2 more advanced, and GBC-3 and −4 the most advanced (***Figure 4B***). Consistent with this developmental trajectory, both GBC-1 and GBC-2 express the early GBC marker *Ascl1* (***Cau et al., 1997***; ***Manglapus et al., 2004***). GBC-1 is likely to be more primitive than GBC-2, based on the frequent and high expression of the later GBC markers *Neurog1* and *Neurod1* (***Cau et al., 1997***; ***Manglapus et al., 2004***) in the latter, not the former (***Figure 4C***). While GBC-3 and −4 are clearly GBCs based on the expression of several GBC markers (e.g. *Neurog1* and *Neurod1*), they also express iOSN markers (e.g. *Gng8* and *Gap43* [***Iwema and Schwob, 2003***; ***Figure 4C***]), consistent with GBC-3 and -4 being iOSN precursors and hence advanced GBCs. iOSNs also segregated into several cell sub-clusters that each express unique genes (***Figure 4D***). These iOSN sub-clusters follow

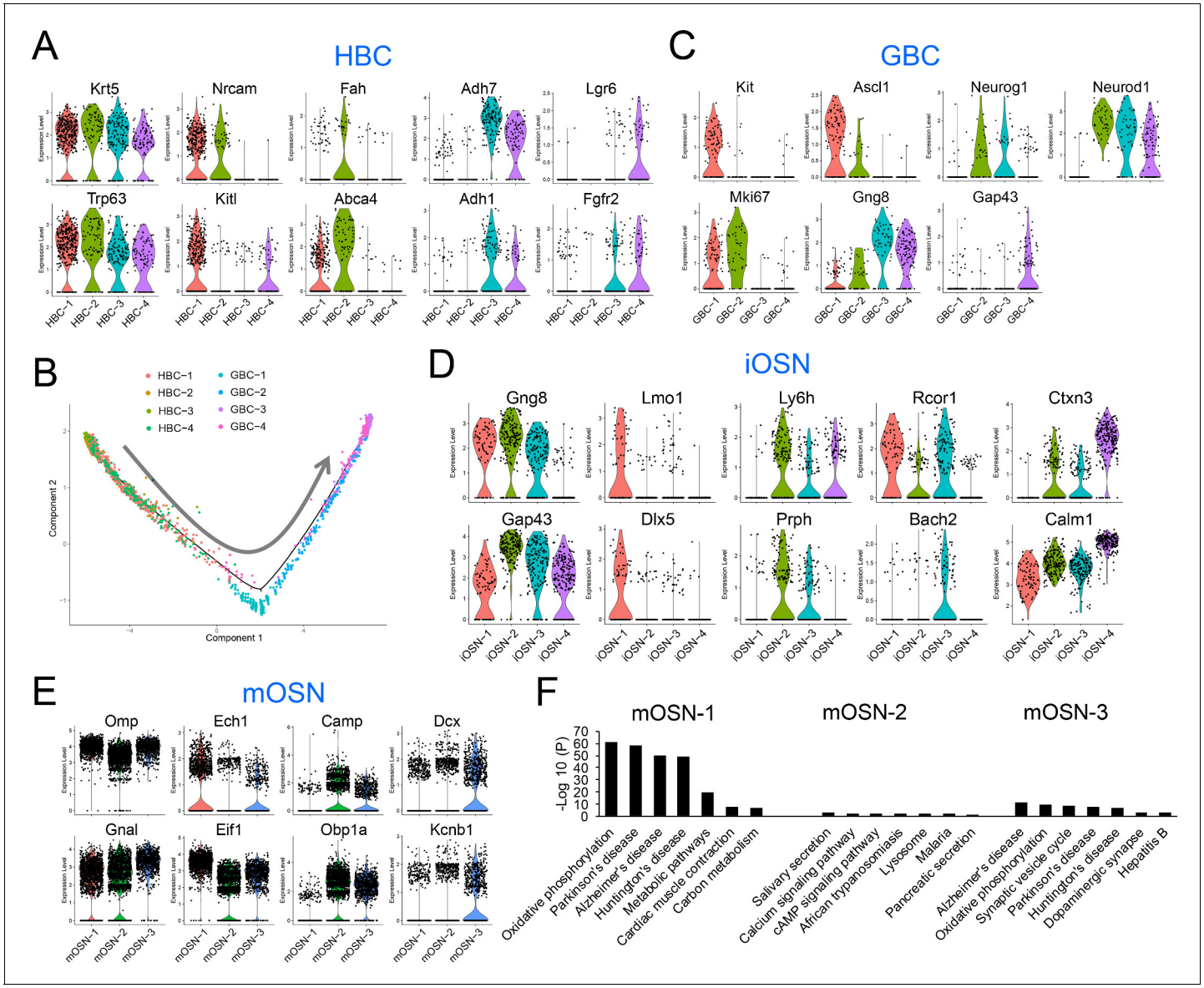

Figure 4. HBC, GBC, iOSN and mOSN heterogeneity. (**A**) Violin plots showing the expression of selective gene markers in the four indicated HBC sub-clusters in WT mice. (**B**) Monocle trajectory analysis of the HBC and GBC sub-clusters we identified. The arrow indicates the inferred direction of differentiation. (**C–E**) Violin plots showing the expression of selective gene markers in the indicated GBC, iOSN, and mOSN sub-clusters in WT mice. (**F**) The most statistically enriched signaling pathways in the mOSN-1,–2, and –3 sub-clusters.

a 'linear' pattern as depicted by the UMAP algorithm (***Figure 3D***), consistent with them representing sequential developmental states, each with unique transcriptomes.

Most WT mOSNs segregated into three different cell clusters (***Figure 3D***), each of which preferentially express different genes (***Figure 4E***). GO and KEGG signaling pathway analyses indicated that these three mOSN sub-clusters are enriched for different functions and signaling pathways, respectively (***Figure 4F***; ***Supplementary file 4***).

OSN molecular pathways

Monocle pseudotime analysis of the OSN precursor/OSN cell clusters indicated that they follow a HBC→GBC→iOSN→mOSN trajectory (***Figure 5A***), consistent with previous studies (***Fletcher et al., 2017***; ***Schwob et al., 2017***; ***Tepe et al., 2018***). To define candidate molecular events occurring during OSN development, we identified genes whose expression is statistically enriched along this

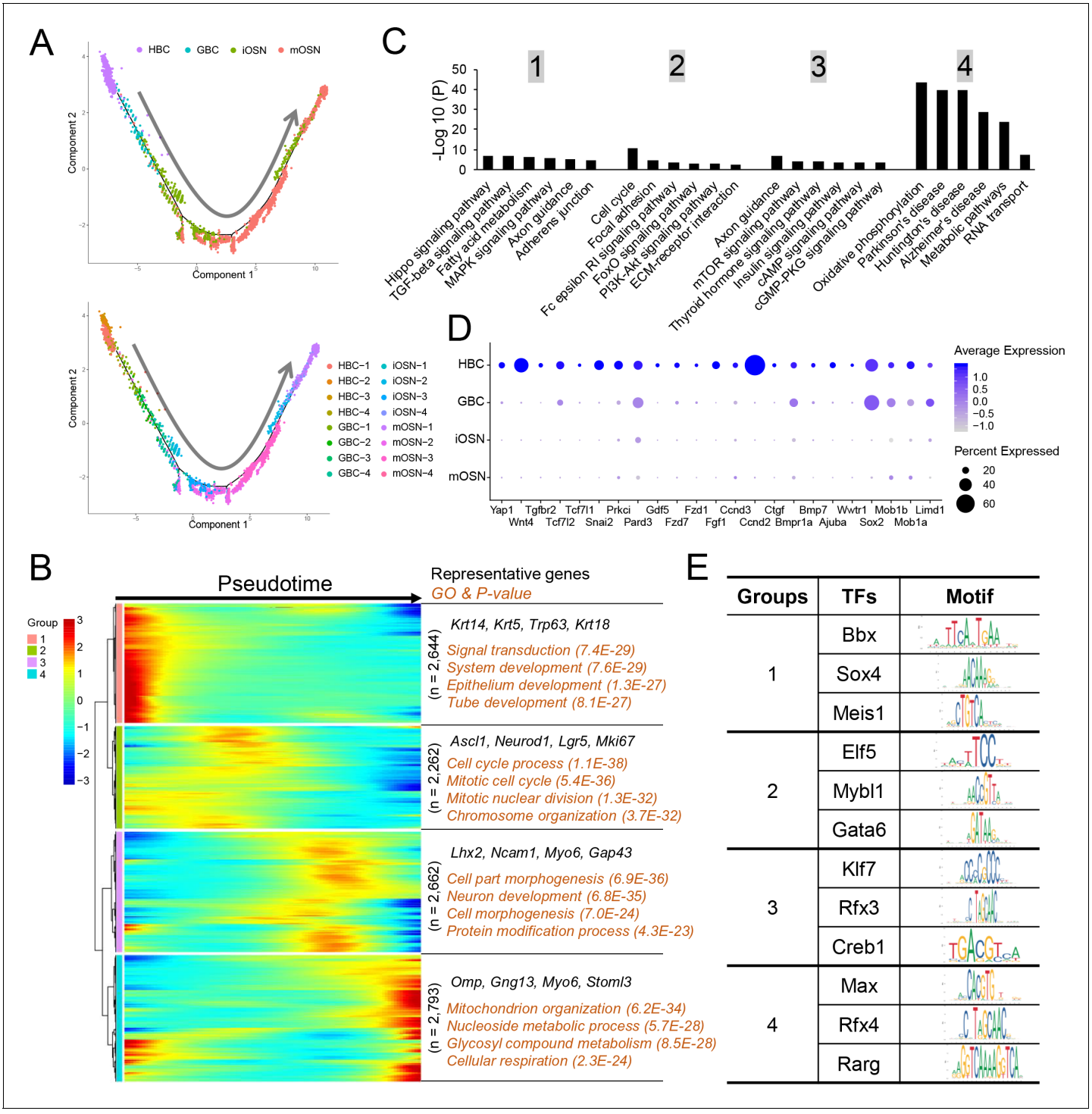

Figure 5. Gene groups exhibiting distinct expression dynamics during OSN development. (**A**) Monocle pseudotime trajectory analysis of the indicated cell clusters and sub-clusters from WT mice defined in ***Figure 3B*** (top) and ***Figure 3D*** (bottom), respectively. (**B**) Heatmap depicting the expression pattern of the four gene groups we defined, each with a unique expression pattern, as defined by the trajectory timeline shown in (**A**), upper. Top: pseudotime directions; right: the number of differentially expressed genes in each group and representative biological processes and P-values. (**C**) The most statistically enriched signaling pathways corresponding to each of the four gene groups defined in (**B**). (**D**) Dot plot showing genes related to the Hippo signaling pathway are primarily expressed in HBCs. (**E**) Transcription factor genes exhibiting the most statistically enriched expression in each gene group defined in (**B**). Target sequences predicted by the ENCODE database are indicated.

pseudotime trajectory (***Supplementary file 4***). This analysis identified 4 distinct patterns of gene expression dynamics that we named groups 1 to 4 (***Figure 5B***). Group-1 genes are dominated by genes expressed transiently in HBCs, including the previously defined HBC-marker genes *Trp63, Krt5,* and *Krt14*. Group-1 genes are statistically enriched for 'signal transduction' and various 'development' categories (***Figure 5B***). Group-2 genes contain GBC genes; indeed the GBC markers *Ascl1*, *Neurod1*, and *Lgr5* are enriched in group 2. 'Cell cycle process' is statistically enriched (***Figure 5B***), consistent with the fact that GBCs undergo self-renewal and proliferative expansion. Group-3 genes are mainly expressed in iOSNs, include the well-established iOSN marker genes *Lhx2, Ncam1*, and *Gap43*. 'Neuron development' is enriched in group 3 (***Figure 5B***), consistent with the fact that iOSNs are undergoing the final stages of development prior to becoming mature neurons. Group-4 genes are mainly expressed in mOSNs; enriched GO categories include 'mitochondrion organization,' 'metabolism,' and 'cellular respiration'.

KEGG signaling pathway analysis revealed that genes involved in different signaling pathways are enriched in each of the 4 groups (***Figure 5C***). For example, Hippo pathway genes are enriched in group 1 (***Figure 5D***), raising the possibility this signaling pathway may be important for maintaining HBC stem cells in the quiescent state or eliciting their activation in response to insults.

We also screened for transcription factors preferentially expressed at different stages of OSN development. We identified 209, 178, 169, and 135 transcription factor genes exhibiting enriched expression in groups 1, 2, 3 and 4, respectively (***Supplementary file 4***). The top 3 transcription factors in each group and their DNA-binding specificity are shown in ***Figure 5E***.

UPF3B impacts HBCs and mOSNs

The array of UPF3B-dependent NMD targets we identified in mOSNs (***Figure 2***) raised the possibility that UPF3B has roles in mOSNs and possibly OSN precursors. To assess this, we first determined whether loss of UPF3B impacts the frequency of HBCs, GBCs, iOSNs, and mOSNs. scRNA-seq analysis revealed that there was a significant reduction in the frequency of HBCs in *Upf3b*-null mice relative to WT mice, when compared to either all OSN precursors/OSNs or all OE cells ($p<0.05$; ***Figure 6A***). As validation, IHC staining with the HBC marker, TRP63, showed that the density of TRP63+ cells was significantly less in *Upf3b*-null OE than WT OE (***Figure 6—figure supplement 1A***). This effect appeared to be specific, as we observed no significant difference in the relative proportion of GBCs, iOSNs, and mOSNs between *Upf3b*-null and WT mice (***Figure 6—figure supplement 1B***). However, we cannot rule out that the variability among the four samples for each genotype might have obscured a subtle change in the fraction of GBCs, iOSNs, or mOSNs in *Upf3b*-null mice. This variability might either be the result of biological differences between individual mice or differences in dissection and/or cell dissociation. However, as further evidence that the overall frequency of mOSNs was not affected in *Upf3b*-null mice, the mOSN marker, OMP, was similarly expressed (at both the RNA and protein levels) in OE from *Upf3b*-null and WT mice, as assessed in OE preparations obtained from different mice (but of the same genotypes) than those used for scRNA-seq analysis (***Figure 1B*** and ***Figure 6—figure supplement 1C***).

Our identification of HBC, GBC, iOSN, and mOSN sub-clusters (***Figure 3D***) gave us an opportunity to elucidate whether UPF3B has a role in this unexpected heterogeneity. Despite no significant effect on the mOSN stage as a whole (***Figure 6—figure supplement 1B***), we observed a striking increase in the frequency of 1 of the 4 mOSN sub-clusters—mOSN-4—in *Upf3b*-null mice (***Figure 6B,C***). This sub-cluster represented <1% of all OSNs in most WT mice and increased by an average of 25-fold in *Upf3b*-null mice ($p<0.05$). Conversely, *Upf3b*-null mice had an almost complete loss of another mOSN sub-cluster—mOSN-2—a sub-cluster that was populated by many cells in most WT mice (***Figure 6B,C***). While this reduction failed to reach statistical significance because of variability between samples ($p=0.24$), it is supported by the independent tSNE plots we generated for *Upf3b*-null vs. WT OSNs (***Figure 3D***). Together these results raise the possibility that a 'mOSN subset switch' occurs in *Upf3b*-null mice. Pearson correlation analysis showed that mOSN-2 and −4 sub-clusters are less related to each other in expression profile than they are to the other two mOSN sub-clusters (***Figure 6—figure supplement 2A***). Indeed, these two mOSN sub-clusters have remarkably distinct molecular characteristics (***Figure 6D*** and ***Supplementary file 4***). Thus, the simultaneous loss and acquisition of these mOSN subsets in *Upf3b*-null mice has the potential to alter olfaction.

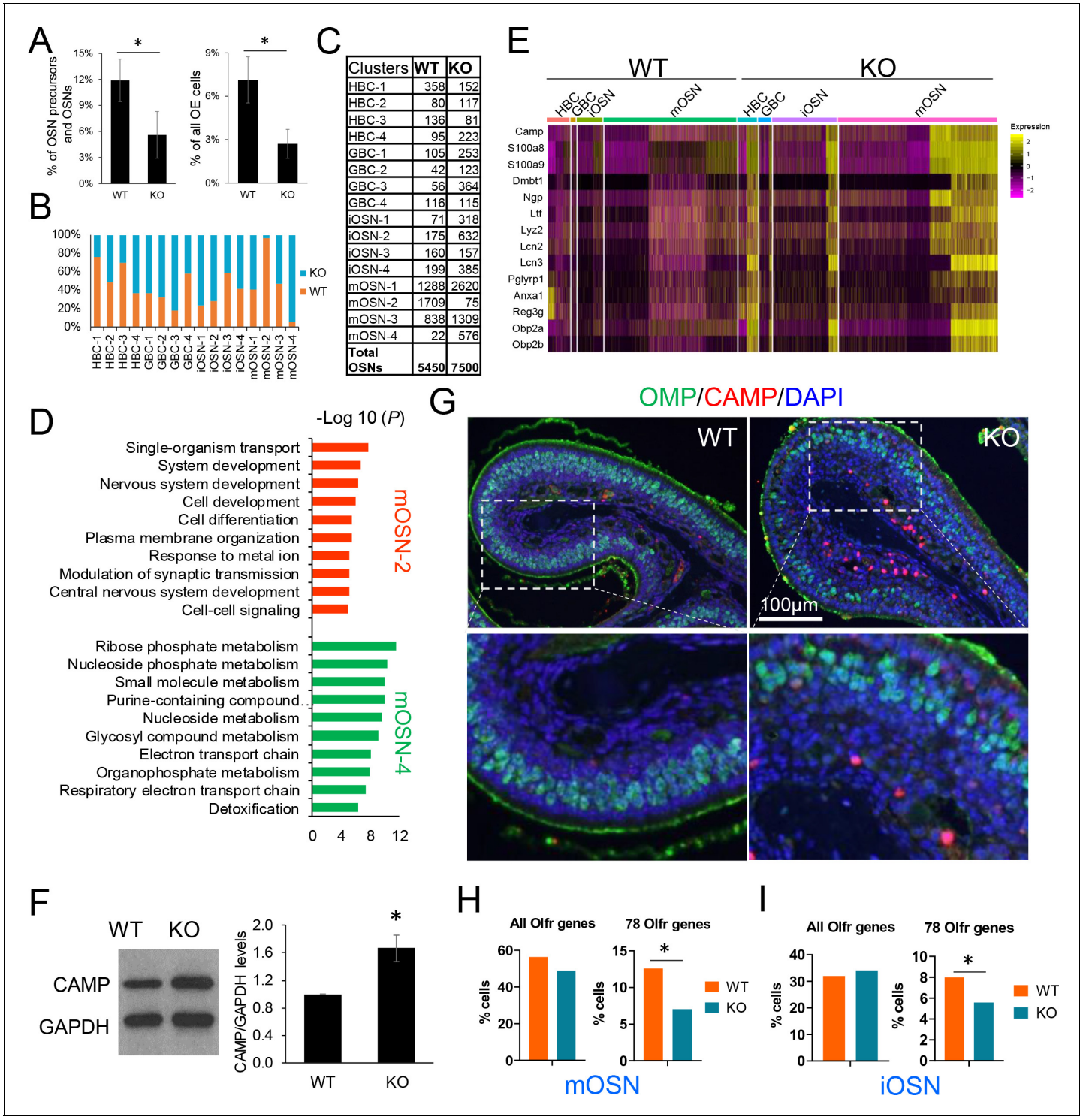

Figure 6. UPF3B shapes olfactory neurogenesis. (**A**) The fraction of HBCs per all OSN precursors/OSNs (HBCs, GBCs, iOSNs and mOSNs) (left) or all OE cells (right), in *Upf3b*-null (KO) and WT mice, as determined by scRNA-seq analysis. *, p<0.05. (**B**) The percentage of cells from the indicated cell sub-clusters in *Upf3b*-null (KO) and WT mice, as determined by scRNAseq analysis. (**C**) Cell number in each cell sub-cluster, as defined in ***Figure 3D***. (**D**) Most statistically enriched GO terms in the mOSN-2 and −4 sub-clusters. (**E**) Heatmap depicting the expression pattern of anti-microbial genes in the indicated cell subsets. (**F**) Left: Western blot analysis of endogenous CAMP protein level in the OE from *Upf3b*-null (KO) and WT mice. Right: quantification of CAMP level normalized against GAPDH (n = 3). *, p<0.05. (**G**) IF analysis of adult mouse OE sections co-stained with antisera against CAMP (red) and OMP (green). Nuclei were stained with DAPI (blue). (**H, I**) The percentage of mOSNs (**H**) and iOSNs (**I**) in our scRNAseq datasets that

Figure 6 continued on next page

Figure 6 continued

express *Olfr* genes. Left, all known *Olfr* genes. Right, the 78 *Olfr* genes significantly downregulated in *Upf3b*-null mice, based on RNAseq analysis (***Figure 1C***). *, p<0.05.

The online version of this article includes the following figure supplement(s) for figure 6:

Figure supplement 1. Impact of UPF3B loss on OE cell subsets.

Figure supplement 2. mOSN subsets and UPF3B-regulated genes.

UPF3B shapes the OLFR repertoire and suppresses immune gene activation

To define genes that are candidates to act downstream of NMD in different OSN cell populations, we used our scRNA-seq datasets to identify genes differentially expressed in the *Upf3b*-null vs. WT cell clusters (***Supplementary file 4***). This revealed that a major category of *Upf3b*-regulated genes in OSNs are immune genes, including a large fraction of genes encoding antimicrobial proteins (***Supplementary file 5***). This was intriguing, as it raised the possibility that OSNs not only normally function in olfaction but also in defense against microbes, a reasonable possibility given that the OE is direct contact with the outside environment. The expression of anti-microbial genes was not confined to the mature neurons in the OE (i.e. mOSNs), as we found that most of these immune-defense genes were also expressed and upregulated in *Upf3b*-null mice at the HBC, GBC, and iOSNs stages (***Figure 6E***). More than half (48 out of 88) of these upregulated mRNAs encoding immune-related proteins harbor at least one NIF (***Supplementary file 5***). This suggests that many of these mRNAs encoding immune system factors are directly targeted for decay by the NMD pathway. This has interesting potential physiological consequences, as described in the Discussion.

Among the antimicrobial genes expressed and upregulated in *Upf3b*-null OSN precursors and OSNs was *Camp* (also known as '*Cramp*'), which encodes a member of the cathelicidin family of antimicrobial peptides that has an important role in the defense against microbial infections, and functions in cell chemotaxis, immune mediator induction, and inflammatory response regulation (***Zhang and Gallo, 2016***). To further assess its regulation, we performed western blot analysis with a validated anti-CAMP antiserum, which showed that CAMP protein is expressed in the OE and is upregulated in *Upf3b*-null mice (***Figure 6F***). As further evidence, immunofluorescence analysis detected modest anti-CAMP staining in OE cells (as well as strong staining in the in the lamina propria), both of which were increased in *Upf3b*-null mice (***Figure 6G*** and ***Figure 6—figure supplement 2B***).

The other major category of genes that we discovered are regulated by *Upf3b* in the OE is *Olfr* genes. As described above, our RNA-seq analysis of purified mOSNs from *Upf3b*-null and WT mice revealed that the *majority* of genes downregulated in response to *Upf3b* loss are *Olfr* genes (***Figure 1C***). In total, we identified 78 *Olfr* genes significantly downregulated in *Upf3b*-null mOSNs (***Figure 1C***). We considered the possibility that these 78 *Olfr* genes are regulated by *Upf3b* through a common local *cis*-acting regulatory sequence, but against this hypothesis, we found that these 78 *Olfr* genes are widely chromosomally distributed (***Figure 6—figure supplement 2C***).

There are more than 1000 olfactory receptor (*Olfr*) genes in mice (***Zhang and Firestein, 2002***). Individual OSNs select a single *Olfr* gene for expression from this large repertoire (***Chess et al., 1994***; ***Malnic et al., 1999***; ***Serizawa et al., 2003***). This unique mechanism raised the possibility that rather than regulating *Olfr* expression per se, *Upf3b* might instead influence the decision whether or not specific *Olfr* genes are selected to be the dominant receptors in mOSNs. In other words, *Upf3b* might increase the probability that these 78 *Olfr* genes that are selected to be expressed in individual mOSNs. If selected less often in *Upf3b*-null OSNs, these 78 *Olfr* genes would appear to be downregulated, but would instead be expressed in fewer OSN. To address this model, we made use of our scRNA-seq datasets. We found that 490 of 3887 mOSNs in WT mice (13%) express one of these 78 *Olfr* genes as the dominant *Olfr* gene. In contrast, only 328 of 4654 mOSNs in *Upf3b*-null mice (7%) express one of these 78 *Olfr* genes as the dominant *Olfr* gene (***Figure 6H***). In contrast, when all known *Olfr* genes were considered as a group, there was no significant difference in the percentage of *Olfr* genes selected in *Upf3b*-null vs. WT mOSNs (***Figure 6H***). Likewise, we found that these 78 *Olfr* genes were under-represented in *Upf3b*-null iOSNs as compared with WT iOSNs (5.6% vs 8.0%, p<0.05) (***Figure 6I***). Together, these results support a model in which UPF3B promotes the

selection of these 78 *Olfr* genes to be the dominant *Olfr* gene expressed in individual mOSNs, a model we elaborate on in the Discussion.

Discussion

NMD factors have been shown to have numerous roles in the development and function of neurons (**Jaffrey and Wilkinson, 2018**). As described in the Introduction, the NMD factor examined in our study – UPF3B – has been shown to be necessary for normal cognition in humans and its loss is associated with several neuro-developmental disorders (**Nguyen et al., 2014**; **Tarpey et al., 2007**). While the precise roles of UPF3B in behaviors is not known, it has been shown that UPF3B is critical for both neural differentiation and mature neuronal functions (**Alrahbeni et al., 2015**; **Huang et al., 2018**; **Jolly et al., 2013**). In addition to *UPF3B*, other NMD genes are likely to have roles in the nervous system (**Jaffrey and Wilkinson, 2018**). For example, copy-number gain and loss of several genes encoding proteins involved in NMD—including *UPF2, UPF3A, SMG6, RBM8A, EIF4A3,* and *RNPS1*—are statistically significantly associated with neural-developmental disorders in humans (**Nguyen et al., 2013**). Mutations in *RBM8A* have been shown to cause TAR syndrome, which can cause cognitive dysfunction (**Jaffrey and Wilkinson, 2018**). In mice, loss of a single copy of *Rbm8a* or other EJC genes (*Magoh* or *Eif4e*) causes microcephaly and severe neural defects (**Mao et al., 2017**). In worms, flies and mice, genetic perturbation of other NMD genes causes neural defects, including synaptic and axon guidance defects (**Colak et al., 2013**; **Giorgi et al., 2007**; **Long et al., 2010**; **Zheng et al., 2012**). Two recent studies revealed that conditional loss of the NMD gene, *Upf2*, in specific neural populations in mice causes a variety of intriguing defects, including aberrant behavior, spine density, and synaptic plasticity (**Johnson et al., 2019**; **Notaras et al., 2019**). Together, these studies make a strong case that NMD has roles in the CNS.

Here, we report the first investigation of the role of NMD in the olfactory system. One of our major findings was that *Upf3b* loss causes shifts in gene expression in OSNs. One major class of genes impacted by *Upf3b* is the *Olfr* genes. These genes have evolved to allow recognition of the large array of odors encountered by higher organisms. In mice, there are >1000 *Olfr* genes, each of which encode a G-coupled receptor that binds to a restricted set of odorants (**Godfrey et al., 2004**; **Zhang and Firestein, 2002**). In order to interpret the information from a given odor, it is critical that only a single OLFR be expressed in each mOSN. This is accomplished by a novel gene regulatory mechanism that selects only a single *Olfr* gene to be expressed in any given mOSN (**Chess et al., 1994**; **Malnic et al., 1999**; **Serizawa et al., 2003**). While the underlying mechanism for this 'one-neuron-one-receptor' rule is not fully understood, a prevailing model is that a stochastic mechanism drives a single *Olfr* to become dominate transcriptionally, a decision that is reinforced by feedback mechanisms (**Dalton et al., 2013**; **Lewcock and Reed, 2004**; **Serizawa et al., 2004**; **Serizawa et al., 2005**).

The first indication that UPF3B might have a role in the selection of *Olfr* genes came from our RNA-seq analysis, which revealed that the *majority* of genes expressed at lower level in *Upf3b*-null mOSNs are *Olfr* genes. In total, we found that 78 *Olfr* genes are statistically downregulated in *Upf3b*-null mOSN. To address mechanism, we performed scRNA-seq analysis and found that these 78 *Olfr* genes are rarely represented as the dominant genes in individual mOSNs in *Upf3b*-null mice. This defect was also present at the iOSN stage, suggesting that *Upf3b* is involved directly or indirectly in determining which *Olfr* gene are selected for dominant expression during OSN development.

A caveat is the OE contains zones enriched for mOSNs expressing particular sets of OLFRs (**Miyamichi et al., 2005**; **Ressler et al., 1994**), and thus even though we made an effort to dissect the entire OE for RNA-seq analysis, it is possible that there is zonal heterogeneity in the samples we analyzed. To reduce this potential bias, we pooled dissociated OE cells from 3 mice for FACS sorting. Confidence that the 78 *Olfr* genes are regulated by *Upf3b* comes from the reproducibility of the regulation in independent samples (**Figure 1C**) and validation by qPCR (**Figure 1—figure supplement 2B**). Furthermore, our single-cell RNA-seq analysis (which analyzed samples different from those analyzed by RNA-seq) verified the regulation of these 78 *Olfr* genes (**Figure 6H**).

How might *Upf3b* influence the selection of this particular set of *Olfr* genes? Given that UPF3B is a NMD factor, it could promote the decay of an mRNA encoding a repressor that acts to regulate the selection of these 78 *Olfr* genes for dominant expression. To test this model, we screened genes

exhibiting significantly upregulated expression in *Upf3b*-null OSNs for those that encode factors known to regulate *Olfr* gene expression or have binding sites in *Olfr* promoters (**Clowney et al., 2011**; **Dalton et al., 2013**; **Hirota and Mombaerts, 2004**; **Markenscoff-Papadimitriou et al., 2014**; **McIntyre et al., 2008**; **Michaloski et al., 2006**; **Wang et al., 1997**). This screen identified two genes—*Mafg* and *Irf8*—that fulfilled this criteria. Both encode transcriptional repressors (**Igarashi et al., 1994**; **Salem et al., 2014**) that bind O/E consensus sites found in *Olfr* gene promoters (**Michaloski et al., 2006**). Thus, *Mafg* and *Irf8* are candidates to act directly downstream of NMD in a regulatory circuit that suppresses the transcription of these 78 Olfr genes. *Mafg* is a member of the Maf subfamily of basic leucine-zipper transcription factor genes that encode small proteins containing a B-ZAP DNA-binding domain, but lack a transactivation domain, and thus members of this family dimerize to form transcriptional repressors (**Igarashi et al., 1994**). MAFG is best known for its ability to regulate globin transcription in erythroid cells; our results raise the possibility that MAFG also functions in OSNs to regulates *Olfr* genes. IRF8 regulates the development hematopoietic cells; its expression in OSNs raises the possibility that this transcription factor also functions in OSNs.

Our findings support a model in which IRF8 and MAFG normally subtly repress the transcription of a subset of *Olfr* genes in OSNs to fine-tune their expression. Our evidence suggests that IRF8 and MAFG are encoded by NMD target mRNAs, so when NMD is disrupted, these transcriptional repressors are overexpressed, leading to reduced expression of their *Olfr* gene targets in developing OSNs. Thus, NMD deficiency would be expected to reduce the probability that these particular *Olfr* genes will be chosen to be the 'dominant *Olfr* gene' in individual mOSNs, which is precisely what we observed in *Upf3b*-null mice.

A non-mutually exclusive possibility is that *Upf3b* dictates the selection of *Olfr* genes by influencing OSN development. In support, several of the genes we found were regulated by *Upf3b* have been reported to play essential roles in neurogenesis, including *Lrp2, Hk2, Notch2, Gdf11, Fos, Ptch1, Spry2*, and *Cwc22*. *Upf3b* could also indirectly influence the *Olfr* repertoire by differentially affecting the survival of OSNs harboring different OLFRs. In support, we found that *Upf3b* loss upregulates *Fos,* which is associated with OSN apoptosis (**Michel et al., 1994**).

The other major class of genes regulated by *Upf3b* in OSNs is antimicrobial genes. This finding, coupled with our finding that OSNs constitutively express these anti-microbial genes (albeit at low levels), suggests that OSNs function not only in olfaction but also in defense against microbes in the bronchial airways. In support, a recent study showed that inflammation causes OSNs to switch from a role in olfaction to immune defense (**Chen et al., 2019**). This raises the interesting possibility that loss of *Upf3b* triggers OE inflammation, which, in turn, diverts OSNs from functioning in olfaction to immune defense, thereby causing deficient olfaction. In support, another recent study reported that NMD disruption causes neuro-inflammation in the central nervous system (**Johnson et al., 2019**). In particular, this study found that *Upf2* conditional knockout in the murine forebrain leads to immune infiltration, coupled with deficits in memory, synaptic plasticity, social, and vocal communication (**Johnson et al., 2019**). Importantly, they found that anti-inflammatory agents partially rescued many of these deficits, indicating that the inflammation is at least partially responsible for the neural defects in these *Upf2*-conditional knockout mice. It will be intriguing to determine whether humans with *UPF3B* mutations also suffer from neuro-inflammation and whether this is responsible for their intellectual disability.

Our finding that loss of UPF3B upregulates a very large number of immune-related genes in OSNs, over half of which encode mRNAs that have NIFs and thus may be direct NMD targets (**Supplementary file 5**), raises the possibility that this 'immune induction' response to NMD inhibition is physiologically important. In this regard, it is notable that some viruses have been shown to inhibit NMD, and, in turn, NMD can inhibit viral infection (**Wachter and Hartmann, 2014**; **Wada et al., 2018**). Coupled with our data, these findings raise the intriguing possibility that the reason that OSNs express high levels of antimicrobial genes in response to NMD inhibition is because this provides a means to cope with infectious agents, particularly those that inhibit NMD as a means to avoid the antiviral actions of NMD.

In addition to NMD inhibition directly upregulating mRNAs encoding immune factors in OSNs, we identified candidate intermediary factors that may act in a circuit to achieve the same aim. In particular, we identified three mRNAs—*Notch2, Bhlhe40,* and *Rac2*—which are high-confidence NMD targets in mOSNs (**Table 1**) that encode factors previously shown to regulate the expression of

many genes encoding inflammatory mediators and antimicrobial proteins (**Dooley et al., 2009**; **Jarjour et al., 2019**; **Shang et al., 2016**).

Our scRNA-seq analysis indicated that *Upf3b* impacts the steady-state frequency of specific OSN precursor and OSN cell subsets. We found that *Upf3b*-null mice have decreased numbers of HBCs, suggesting that UPF3B promotes the maintenance of these reserve stem cells. This effect appeared to be specific, as we observed no significant effects on GBCs, which also serve as olfactory stem cells, but unlike HBCs, function to generate new mOSNs constitutively (**Schwob et al., 2017**). We also observed that *Upf3b*-null mice acquired a specific group of mOSNs harboring a unique transcriptome that are hardly present in WT mice. This mOSN-4 sub-cluster is enriched for many genes, such as *Tuba1a, Nsg1, Chchd10, Eml2, Ubb,* and *Gldc*, which suggests that *Upf3b* normally represses these genes. It remains to be determined whether the aberrant over-expression of these genes causes aberrant mOSN function. We also found that *Upf3b*-null mice largely lack a mOSN sub-cluster—mOSN-2—that we found contained large numbers of cells in most WT mice. The mOSN-2 sub-cluster is likely to be functional, as genes enriched in this sub-cluster include *Pten, App, Cnga2, Nrp2, Ncam1, Adcy3, Gnal, Atf5*, and *Gfy* (**Supplementary file 4**), all of which are known to be essential for olfactory epithelium development and/or olfaction. This reciprocal shift in these two mOSN sub-clusters in *Upf3b*-null mice raises the possibility that UPF3B loss converts the mOSN-2 sub-cluster into the mOSN-4 sub-cluster. This remains to be determined, as does the physiological consequences of these shifts in mOSN sub-populations. Another important area for future investigation is to determine whether these cell-subset alterations in *Upf3b*-null mice are cell autonomous or non-cell autonomous.

As described in the Introduction, few direct NMD target RNAs have previously been defined in vivo. Our study fills this gap by identifying high-confidence NMD target mRNAs in mOSNs in vivo. Many of the NMD targets we identified in mOSNs have long 3'UTRs, raising the possibility that mOSNs have a predilection for degrading mRNAs with this particular NIF. By analogy, evidence suggests that mRNAs harboring long 3'UTRs are also preferentially targeted for destruction by NMD in male germ cells (**Bao et al., 2016**). Several of the NMD target mRNAs that we identified in mOSNs are good candidates to have roles in OSN development. For example, *Gdf11* functions in negative-feedback control of OE neurogenesis; *Lrp2* promotes the proliferation of neural precursor cells in the subependymal zone of the olfactory bulb; and *Notch2* is required for maintaining sustentacular cell function in the OE (**Gajera et al., 2010**; **Kawauchi et al., 2009**; **Rodriguez et al., 2008**). Other NMD target mRNAs that we identified, including *Ptch1* and *Hk2,* encode proteins known to be important for the development of neurons outside of the olfactory system (**Iulianella and Stanton-Turcotte, 2019**; **Zheng et al., 2016**).

Our study provides a useful resource for the olfactory field. For example, our scRNA-seq analysis identified putative new OSN precursor and OSN cell subsets. While we do not know the significance of this heterogeneity, the genes differentially expressed by the sub-clusters we identified suggests functional relevance. For example, the genes differentially expressed by the 4 cell-sub clusters we identified for both GBCs and iOSNs suggested that these sub-clusters represent distinct developmental stages. Our results are consistent with Fletcher et al., who demonstrated that that the 1 GBC and 4 INP/iOSN sub-clusters they identified follow a linear developmental pattern (**Fletcher et al., 2017**). Our genome-wide determination of mOSN mRNA expression levels and ribosome occupancy (i.e. translation rates) will be useful for future studies to determine how transcription, translation, and other post-transcriptional processes coordinate to regulate the expression of large sets of genes in mature neurons in vivo. We divided mOSN-expressed mRNAs into nine categories based on steady-state mRNA level and ribosome occupancy, allowing dissection of common functions encoded by similarly regulated mRNAs. Given that translation is a highly energy-consuming process (**Lynch and Marinov, 2015**), it is likely that there has been strong selection pressure for many mRNAs to be translated inefficiently. Indeed, we found that modestly translated mRNAs encode many key mOSN proteins, including receptors, signaling factors, and developmental regulators.

In conclusion, our study provides an invaluable set of resources for the olfactory field and identifies a post-transcriptional regulatory pathway that impacts OSNs.

Materials and methods

Key resources table

Reagent type (species) or resource	Designation	Source or reference	Identifiers	Additional information
Gene (*Mus musculus*)	*Upf3b*	GenBank	Gene ID: 68134	
Genetic reagent (*Mus. musculus*)	C57BL/6J	Jackson Laboratory	Stock #: 000664 RRID:MGI:3028467	
Genetic reagent (*Mus. musculus*)	*Upf3b*-null mice	PMID:21925383	RRID:MGI:6110148	Miles Wilkinson lab
Genetic reagent (*Mus. musculus*)	*R26-eYFP* mice	PMID:11299042		Obtained from Dr. Maike Sander (UCSD)
Genetic reagent (*Mus. musculus*)	*Omp-Cre* mice	PMID:22057188		Obtained from Dr. Haiqing Zhao (Johns Hopkins University)
Genetic reagent (*Mus. musculus*)	*RiboTag* mice	PMID:19666516		Obtained from Dr. Paul Ameiux (University of Washington)
Antibody	Rabbit monoclonal anti-OMP (EPR19190)	Abcam	Cat# ab183947 RRID:AB_2858281	IF (1:400), WB (1:2000)
Antibody	Goat polyclonal anti-OMP	FUJIFILM Wako Chemicals	Cat# 544–10001-WAKO RRID:AB_2315007	IF (1:200)
Antibody	Rabbit polyclonal anti-CAMP	Generated by Richard L. Gallo laboratory	PMID:11442754	IF (1:200)
Antibody	Rabbit polyclonal anti-FUT10	Proteintech	Cat#: 18660–1-AP RRID:AB_10641997	IF (1:200)
Antibody	Donkey anti-Goat IgG (H+L) Cross-Adsorbed Secondary Antibody, Alexa Fluor 488	Thermo Fisher Scientific	Cat#: A-11055 RRID:AB_2534102	IF (1:1000)
Antibody	Donkey anti-Rabbit IgG (H+L) Highly Cross-Adsorbed Secondary Antibody, Alexa Fluor 555	Thermo Fisher Scientific	Cat#: A-31572 RRID:AB_162543	IF (1:1000)
Sequence-based reagent	Fosl2_F	This paper	PCR primers	CCGCAGAAGGAGAGATGAG (from IDT)
Sequenced-based reagent	Fosl2_R	This paper	PCR primers	GCAGCTTCTCTGTCAGCTC (from IDT)
Sequence-based reagent	Ptger2_F	This paper	PCR primers	TGCTCCTTGCCTTTCACAATC (from IDT)
Sequenced-based reagent	Ptger2_R	This paper	PCR primers	CCTAAGTATGGCAAAGACCCAAG (from IDT)
Sequence-based reagent	Adcy6_F	This paper	PCR primers	TTCCTGACCGTGCCTTCTC (from IDT)
Sequenced-based reagent	Adcy6_R	This paper	PCR primers	CACCCCGGTTGTCTTTGC (from IDT)
Sequence-based reagent	Ptch1_F	This paper	PCR primers	ACCTCCTAGGTAAGCCTCC (from IDT)
Sequenced-based reagent	Ptch1_R	This paper	PCR primers	CACCCACAATCAACTCCTCC (from IDT)
Sequence-based reagent	Cwc22_F	This paper	PCR primers	CAGAAGACAGATACACAGAGCAAG (from IDT)

Continued on next page

Continued

Reagent type (species) or resource	Designation	Source or reference	Identifiers	Additional information
Sequenced-based reagent	Cwc22_R	This paper	PCR primers	CTCTCTCTCTCTCTCTGCGTTT (from IDT)
Sequence-based reagent	Fut10_F	This paper	PCR primers	CCAGGGCCTTCCTATTCTACG (from IDT)
Sequenced-based reagent	Fut10_R	This paper	PCR primers	CTGAATGTGGCCGTATGGTTG (from IDT)
Sequence-based reagent	Gdpd3_F	This paper	PCR primers	TGATCCGACACTTGCAGGAC (from IDT)
Sequenced-based reagent	Gdpd3_R	This paper	PCR primers	GCTGTGGGGTAATCGGTCAT (from IDT)
Sequence-based reagent	Olfr827_F	This paper	PCR primers	TGGGATGGTTCTTCTGGGAA (from IDT)
Sequenced-based reagent	Olfr827_R	This paper	PCR primers	ACCGTGGAGTAGGAGAGGTC (from IDT)
Sequence-based reagent	Rpl19_F	This paper	PCR primers	CCTGAAGGTCAAAGGGAATGTG (from IDT)
Sequenced-based reagent	Rpl19_R	This paper	PCR primers	CTTTCGTGCTTCCTTGGTCTT (from IDT)
Commercial assay or kit	Chromium Single Cell 3' Library and Gel Bead Kit	10X Genomics	Cat# 120237	
Commercial assay or kit	iScript cDNA synthesis Kit	BioRad	Cat# 170–8891	
Commercial assay or kit	SsoAdvanceD Universal SYBR Green Supermix	BioRad	Cat# 172–5274	
Commercial assay or kit	RNeasy Mini Kit	Qiagen	Cat# 74104	
Software, algorithm	Cell Ranger Version 2.1.1	10x genomics	Cell Ranger Version 2.1.1	
Software, algorithm	Seurat (v3.1.5)	Designed by Rahul Satija laboratory	PMID:31178118	
Software, algorithm	Monocle (v2.16.0)	Designed by Cole Trapnell laboratory	PMID:28114287	
Software, algorithm	NIH ImageJ (v1.8.0)	NIH	Version 1.8.0	

Mice

This study was carried out in strict accordance with the Guidelines of the Institutional Animal Care and Use Committee (IACUC) at the University of California, San Diego. The protocol was approved by the IACUC at the University of California, San Diego (permit number: S09160). All studies were conducted on adult male mice housed under a 12 hr light:12 hr dark cycle and provided with food and water ad libitum. Of note, we only performed analyses on male mice. Since *Upf3b* is X-linked gene, we analyzed Upf3b$^{+/y}$ (WT) and Upf3$^{-/y}$ (KO) mice. All mouse strains used for analysis were backcrossed to C57BL/6J for at least eight passages.

Behavioral and weight analyses

To assess the effect of UPF3B loss on mouse weight, 19male pups (nine *Upf3b*-null and ten WT mice) from *Upf3b*$^{+/-}$ × WT breeders (6 litters) were assessed, performed as described previously (***Tan et al., 2016***). For pre-weaning pups, to reduce stress, forceps and gloves were changed frequently between cages.

For the coyote/bobcat urine experiment, 10 male mice (10- to 16 weeks of age) from each genotype were analyzed. Each mouse was placed into a cage for 10 min to acclimatize, a strip of filter

paper soaked with coyote urine (Snow Joe) or bobcat urine (Predator Pee) was placed into the cage for 5 min, and the amount of time the mouse was in the vicinity of the filter paper was determined by video recording. Each mouse was tested separately in the absence of humans or other mice in the room.

RNA-seq analysis

For each mOSN sample analyzed, 3 C57BL/6J male mice (8- to 9-weeks old) were pooled. Four replicate samples were analyzed per genotype (*Upf3b$^{+/y}$; Omp-Cre; R26-eYFP* and *Upf3b$^{-/y}$; Omp-Cre; R26-eYFP*). Cell sorting experiments were performed on two separate days, with two samples sorted per day. The OE was dissected as described (**Gong, 2012**) and dissociated using the Papain Dissociation System (Worthington) at 37˚C for 15 min, followed by extensive trituration. Cells were filtered using a 40-µm strainer (Falcon). After spinning at 200 *g* for 5 min, cells were resuspended in Hanks' balanced salt solution (HBSS) containing 3% FBS (Gibco) but without Ca^{2+} and Mg^{2+}. The cell suspension was mixed with propidium iodide (final concentration of 1 µg/ml) and the OMP-eYFP^{+} cells were sorted by flow-cytometry. RNA was isolated from the OMP-eYFP^{+} cells using TriZOL (Life Technologies), followed by a secondary purification step using a RNeasy column (Qiagen). Total RNA was assessed for quality using an Agilent Bioanalyzer, and samples determined to have an RNA Integrity Number (RIN) of at least 8 or greater were used to generate RNA libraries using Illumina's TruSeq RNA Sample Prep Kit, following the manufacturer's specifications, with the RNA fragmentation time adjusted to 5 min. RNA-seq was performed at the Institute of Genomic Medicine at UCSD. RNA libraries were multiplexed and sequenced with 100 base pair (bp) pair end reads on an Illumina HiSeq4000. The average number of reads per sample ranged from approximately 15 to 22 million reads. Reads were filtered for quality and aligned with STAR (2.5.2b) against *Mus musculus* release-90, Ensembl genome (GRCm38). The exon counts were aggregated for each gene to build a read count table using SubRead function featureCounts (**Liao et al., 2014**). Using the exon start/end positions, we extracted the exon sequences from the mm10 mouse genome, and ligated them together in silico for each transcript. For each entry, the entire transcript sequence was subtracted from the known CDS sequence (obtained as above) to identify 3'UTR length. DEGs were defined using DESeq2 (**Love et al., 2014**) using a threshold *q*-val of <0.05. The R package program 'pheatmap' was used for clustering and to generate heatmap plots. GO analysis was done using database for annotation, visualization and integrated discovery (DAVID), version v6.8. To infer relative RNA stability, we used the REMBRANDTS program (**Alkallas et al., 2017**) following the tutorial (https://github.com/csglab/REMBRANDTS).

RiboTag analysis

For each mOSN sample analyzed, three C57BL/6J male mice (8 to 9-weeks old) were pooled. Three replicate samples were analyzed per genotype (*Upf3b$^{+/y}$; Omp-Cre; RiboTag* and *Upf3b$^{-/y}$; Omp-Cre; RiboTag*). The OEs was dissected as described (**Gong, 2012**), homogenized, washed with HBSS, centrifuged at 16,000 *g* at 4˚C for 10 min, the supernatant was transferred into a new tube and incubated with HA antisera (#16B12; BioLegend, CA) at 4˚C for 2.5 hr. Ribosome-bound RNAs were captured on anti-HA agarose beads (Pierce) for 1 hr at 4˚C on a tube rotator. RNA libraries were multiplexed and sequenced with 50 bp single-end reads on an Illumina HiSeq4000. RNA sequencing, alignment, and downstream analyses were done as described above for RNA-seq analysis. TE was determined by dividing RiboTag reads by RNA-seq reads. Log2-transformed transcripts per million (TPM) values were used to segregate mRNAs into different categories.

scRNA-seq analysis

Four C57BL/6J male mice (7 to 8-weeks old) per genotype (*Upf3b$^{+/y}$* and *Upf3b$^{-/y}$*) were used to obtain OE for scRNA-seq analysis. After dissecting the OE as described (**Gong, 2012**), the cells were dissociated following the 10X Genomics Chromium sample preparation protocol. Briefly, tissue was cut into 1 mm^3 pieces and digested in HBSS without Ca^{2+} and Mg^{2+} and supplemented with 44 U/ml Dispase (Invitrogen), 1000 U/ml Collagenase type II (Invitrogen) and 10 mg/ml DNaseI (Sigma), for 20 min at 37˚C with gentle agitation. The digested tissue was centrifuged at 300 rcf for 5 min and washed in HBSS without Ca^{2+} and Mg^{2+}. Dissociated cells were resuspended in 3% FBS in PBS. Dead cells were removed using the ClioCell Dead Cell Removal kit (Amsbio) following the

manufacturer's instructions. Single cells were resuspended in 0.04% BSA in PBS (w/v) and loaded on the 10x Chromium chip. Cell capturing, and library preparation was carried as per kit instructions (Chromium Single Cell Kit [v2 chemistry]). The resultant libraries were size selected, pooled, and sequenced using 2 × 100 paired-end sequencing protocol on an Illumina HiSeq 4000 instrument. The libraries initially underwent shallow sequencing to access quality and to adjust subsequent sequencing depth based on the capture rate and unique molecular indices (UMI) detected. All sequencing analyses were performed at the Institute of Genomic Medicine at UCSD.

As described previously (**Sohni et al., 2019**; **Tan et al., 2020b**; **Tan et al., 2020a**), de-multiplexed raw sequencing reads were processed and mapped to the mouse genome (mm10) using Cell Ranger software (v2.0) with default parameters. We filtered raw count matrices by excluding cells expressing less than 200 detectably expressed genes and genes expressed in less than 3 cells. Each library was tagged with a library batch ID and combined across independent experiments using the Seurat package (**Butler et al., 2018**) in R. To check the quality of the single-cell data and to remove multiplets, we performed Seurat-based filtering of cells based on three criteria: number of detected features (nFeature_RNA) per cell, number of UMIs expressed per cell (nCount_RNA) and mitochondrial content, using the following threshold parameters: nFeature_RNA (>500), nCount_RNA (>1,500), and percentage of mitochondrial genes expressed (<0.2%). We used known lineage marker profiles to exclude cell multiplets (cells expressing different lineage markers) and cell-free droplets. Gene expression values were log normalized and regressed by mitochondrial expression ('percent.mt') and cell cycle gene expession ('S.Score' and 'G2M.Score') using the *SCTransform* function. Batch correction was performed using the *JackStraw* functions in the Seurat package.

To identify cell clusters, we employed the UMAP algorithm (**Becht et al., 2019**). The *FindMarkers* function (a Wilcoxon rank sum test) was used to determine differential gene expression between clusters (set at minimum expression in 25% of cells). The *DoHeatmap* function was used to generate an expression heatmap for specific cells and features. GO analysis (DAVID v6.8) was done using the top differentially (positively) expressed genes, with a p-adjusted cut off of 0.01.

Single-cell pseudotime trajectories were constructed with the Monocle two package (v2.10.1) (**Qiu et al., 2017**) according to the provided documentation (http://cole-trapnell-lab.github.io/monocle-release/). UMI counts were modeled as a negative binomial distribution. The ordering genes were identified as having high dispersion across cells (mean_expression >= 0.01; dispersion_empirical >= 1). The discriminative dimensionality reduction with trees (DDRTree) method was used to reduce data to two dimensions. Differentially expressed genes were identified and used for dynamic trajectory analysis (NO discovery rate [FDR]<0.01) to order cells in pseudotime. The *plot_pseudotime_heatmap* function was used to generate heatmaps.

NIF analysis

To define NIFs, Refseq-defined transcripts were first converted into Ensemble transcript IDs and their sequences were obtained using the UCSC Table Browser. NIFs were identified in these transcripts using an algorithm written in Python 2.7, Zenith.py, created by the Wilkinson laboratory. Only transcripts with a detectable 5'UTR and 3'UTR were considered. A transcript was defined as harboring a dEJ if it contained at least one exon-exon junction ≥50 nt downstream of the stop codon terminating the main ORF. A transcript was defined as harboring an uORF if the following criteria were met: (i) the ORF is in the 5' UTR, (ii) the start codon and surrounding nts are in a context known to initiate translation (a purine at the −3 position or a guanine at the +4 position, relative to the A in the AUG initiation codon [+1]) (**Kozak, 1986**), (iii) the ORF is ≥30 nt long, and (iv) the ORF does not overlap with the main ORF (to reduce the probability that translation could be re-initiated, thereby allowing the transcript to escape NMD).

Immunofluorescence analysis

Adult mice were anesthetized and perfused with 4% paraformaldehyde (PFA; Sigma). OE was dissected and fixed in 4% PFA at 4˚C for 24 hr, then transferred to 70% ethanol. After embedding in paraffin, 5 µM sections were prepared, deparaffinized 2 times in xylene, followed by serial dilutions of ethanol. Unmasking was performed with IHC-TekTM epitope retrieval solution using a steamer (IHCWORLD) for 40 min. Blocking was performed by incubating with 5% serum (from the species that the secondary antibody was raised in) for 1 hr at room temperature. The sections were then

incubated overnight with the primary antibody (goat polyclonal OMP, rabbit anti-CAMP [*Gallo et al., 1997*]) at 4˚C and incubated with secondary antibody (Donkey anti-Goat IgG [H+L] conjugated with Alexa Fluor 488 or Donkey anti-Rabbit IgG [H+L] conjugated with Alexa Fluor 555) for 1 hr at room temperature. The nuclei were counterstained with DAPI, and a coverslip was placed over the sections with mounting medium.

Western blot analysis

OEs were incubated in radioimmunoprecipitation assay (RIPA) buffer (Bio-Rad) supplemented with protease inhibitor cocktail (Sigma) on ice for 30 min, followed by centrifugation at 16,000 *g* for 15 min at 4˚C. The lysates were then transferred to new tubes, and protein level was quantified using the DC Protein Assay kit (Bio-Rad). Twenty micrograms of the protein samples were separated on an 15% polyacrylamide gel, and Western blot analysis was performed as previously described (*Ramaiah et al., 2019*). Quantification of the blots was performed using NIH ImageJ (1.8.0).

Acknowledgements

We thank the UCSD Institute for Genomic Medicine for technical support and the San Diego Supercomputer Center for providing data analysis resources. We are grateful to Drs. Maike Sander (UCSD), Haiqing Zhao (Johns Hopkins University), and Paul Ameiux (University of Washington) for providing R26-eYFP, *Omp-Cre*, and RiboTag mice, respectively.

Additional information

Funding

Funder	Grant reference number	Author
Eunice Kennedy Shriver National Institute of Child Health and Human Development	R01 HD093846	Miles F Wilkinson

The funders had no role in study design, data collection and interpretation, or the decision to submit the work for publication.

Author contributions

Kun Tan, Resources, Data curation, Formal analysis, Validation, Writing - original draft; Samantha H Jones, Conceptualization, Data curation; Blue B Lake, Jennifer N Chousal, Formal analysis; Eleen Y Shum, Conceptualization; Lingjuan Zhang, Song Chen, Abhishek Sohni, Shivam Pandya, Data curation; Richard L Gallo, Kun Zhang, Heidi Cook-Andersen, Supervision; Miles F Wilkinson, Conceptualization, Supervision, Funding acquisition, Project administration, Writing - review and editing

Author ORCIDs

Kun Tan https://orcid.org/0000-0002-8567-7795
Blue B Lake http://orcid.org/0000-0002-8637-9044
Song Chen http://orcid.org/0000-0001-5286-3084
Miles F Wilkinson https://orcid.org/0000-0002-6416-3058

Ethics

Animal experimentation: This study was carried out in strict accordance with the Guidelines of the Institutional Animal Care and Use Committee (IACUC) at the University of California, San Diego. The protocol was approved by the IACUC at the University of California, San Diego (permit number: S09160).

Decision letter and Author response

Decision letter https://doi.org/10.7554/eLife.57525.sa1
Author response https://doi.org/10.7554/eLife.57525.sa2

Additional files

Supplementary files

- Supplementary file 1. Quality control matrices of Upf3b-null and control mOSNs RNA-seq datasets. (**1**) QC metrics, (**2**) reads count, and (**3**) TPM values from *Upf3b*-null (KO) and control (WT) mOSN RNA-seq and RiboTag datasets. (**4**) The expression of all annotated *Olfr* genes in *Upf3b*-null (KO) and control (WT) mOSN samples, based on RNA-seq analysis.
- Supplementary file 2. mOSN transcriptome, translome, and NMD targets. (**1**) Genes differentially expressed between *Upf3b*-null and WT mOSNs (as defined by RNA-seq analysis), including their known NIFs. (**2**) High-confidence NMD targets: transcripts both upregulated and stabilized in *Upf3b*-null mOSNs. (**3**) The transcriptome and translome of *Upf3b*-null and WT mOSNs, based on RNA-seq and RiboTag analyses. (**4**) Translational efficiency (TE) of RNAs expressed in *Upf3b*-null and WT mOSNs, as defined by RNA-seq and RiboTag analyses.
- Supplementary file 3. Putative mouse NMD target RNAs defined by previous studies.
- Supplementary file 4. Genes exhibiting enriched expression in scRNA-seq-defined OE cell subsets. (**1**) Genes exhibiting enriched expression in all OE cell types identified by scRNA-seq analysis. (**2**) Genes exhibiting enriched expression in HBC, GBC, iOSN, and mOSN sub-clusters identfied by scRNA-seq analysis. (**3**) Genes exhibiting enriched expression in the 4 temporally distinct gene groups defined by pseudotime trajectory analysis of HBCs, GBCs, iOSNs, and mOSNs. (**4**) Transcription factor (TF) genes exhibiting enriched expression in the 4 temporally distinct gene groups defined by pseudotime trajectory analysis of HBCs, GBCs, iOSNs, and mOSNs.
- Supplementary file 5. Immune genes expressed in HBCs, GBCs, iOSNs, and mOSNs. (**1**) Immune genes enriched in *Upf3b*-null HBC, GBC, iOSN, and mOSN sub-clusters identified by scRNA-seq analysis. (**2**) NIFs present in immune genes expressed in *Upf3b*-null OSNs.
- Transparent reporting form

Data availability

Sequencing data have been deposited in GEO under accession code GSE146043.

The following dataset was generated:

Author(s)	Year	Dataset title	Dataset URL	Database and Identifier
Tan K, Jones SH, Wilkinson MF	2020	The role of the NMD factor UPF3B in olfactory sensory neurons	https://www.ncbi.nlm.nih.gov/geo/query/acc.cgi?acc=GSE146043	NCBI Gene Expression Omnibus, GSE146043

The following previously published datasets were used:

Author(s)	Year	Dataset title	Dataset URL	Database and Identifier
Hurt JA, Robertson AD, Burge CB	2013	Global Analyses of UPF1 Binding and Function Reveal Expanded Scope of Nonsense-Mediated mRNA Decay	https://www.ncbi.nlm.nih.gov/geo/query/acc.cgi?acc=GSE41785	NCBI Gene Expression Omnibus, GSE41785
Mao H, McMahon JJ, Tsai YH, Wang Z, Silver DL	2016	Haploinsufficiency for Core Exon Junction Complex Components Disrupts Embryonic Neurogenesis and Causes p53-Mediated Microcephaly	https://www.ncbi.nlm.nih.gov/geo/query/acc.cgi?acc=GSE85576	NCBI Gene Expression Omnibus, GSE85576
Mooney CM, Jimenez-Mateos EM, Engel T, Mooney C, Diviney M, Venø MT, Kjems J, Farrell MA, O'Brien DF, Delanty N, Henshall DC	2017	RNA sequencing of synaptic and cytoplasmic Upf1-bound transcripts supports contribution of nonsense-mediated decay to epileptogenesis	https://doi.org/10.1038/srep41517	RNA sequencing of synaptic and cytoplasmic Upf1-bound transcripts supports contribution of nonsense-mediated decay to epileptogenesis, 10.

				1038/srep41517
Bao j, Vitting-Seerup K, Waage J, Tang C, Ge Y, Porse BT, Yan W	2016	UPF2-Dependent Nonsense-Mediated mRNA Decay Pathway Is Essential for Spermatogenesis by Selectively Eliminating Longer 3'UTR Transcripts	https://www.ncbi.nlm.nih.gov/geo/query/acc.cgi?acc=GSE55180	NCBI Gene Expression Omnibus, GSE55180
McIlwain DR, Pan Q, Reilly PT, Elia AJ, McCracken S, Wakeham AC, Itie-Youten A, Blencowe BJ, Mak TW	2010	Smg1 is required for embryogenesis and regulates diverse genes via alternative splicing coupled to nonsense-mediated mRNA decay	https://doi.org/10.1073/pnas.1007336107	Smg1 is required for embryogenesis and regulates diverse genes via alternative splicing coupled to nonsense-mediated mRNA decay, 10.1073/pnas.1007336107
Weischenfeldt J, Damgaard I, Bryder D, Theilgaard-Mönch K, Thoren LA, Nielsen FC, Jacobsen SEW, Nerlov C, Porse BT	2008	NMD Is Essential for Hematopoietic Stem and Progenitor Cells and for Eliminating By-Products of Programmed DNA Rearrangements10.1101/gad.468808	NMD Is Essential for Hematopoietic Stem and Progenitor Cells and for Eliminating By-Products of Programmed DNA Rearrangements, 10.1101/gad.468808	
Thoren LA, Nørgaard GA, Weischenfeldt J, Waage J, Jakobsen JS, Damgaard I, Bergström FC, Blom AM, Borup R, Bisgaard HC, Porse BT	2010	UPF2 Is a Critical Regulator of Liver Development, Function and Regeneration	https://doi.org/10.1371/journal.pone.0011650	UPF2 Is a Critical Regulator of Liver Development, Function and Regeneration, 10.1371/journal.pone.0011650

References

Alkallas R, Fish L, Goodarzi H, Najafabadi HS. 2017. Inference of RNA decay rate from transcriptional profiling highlights the regulatory programs of Alzheimer's disease. *Nature Communications* **8**:909. DOI: https://doi.org/10.1038/s41467-017-00867-z, PMID: 29030541

Alrahbeni T, Sartor F, Anderson J, Miedzybrodzka Z, McCaig C, Müller B. 2015. Full UPF3B function is critical for neuronal differentiation of neural stem cells. *Molecular Brain* **8**:33. DOI: https://doi.org/10.1186/s13041-015-0122-1, PMID: 26012578

Bao J, Vitting-Seerup K, Waage J, Tang C, Ge Y, Porse BT, Yan W. 2016. UPF2-Dependent Nonsense-Mediated mRNA decay pathway is essential for spermatogenesis by selectively eliminating longer 3'UTR Transcripts. *PLOS Genetics* **12**:e1005863. DOI: https://doi.org/10.1371/journal.pgen.1005863, PMID: 27149259

Barrett LW, Fletcher S, Wilton SD. 2012. Regulation of eukaryotic gene expression by the untranslated gene regions and other non-coding elements. *Cellular and Molecular Life Sciences* **69**:3613–3634. DOI: https://doi.org/10.1007/s00018-012-0990-9, PMID: 22538991

Bear DM, Lassance JM, Hoekstra HE, Datta SR. 2016. The evolving neural and genetic architecture of Vertebrate Olfaction. *Current Biology* **26**:R1039–R1049. DOI: https://doi.org/10.1016/j.cub.2016.09.011, PMID: 27780046

Becht E, McInnes L, Healy J, Dutertre C-A, Kwok IWH, Ng LG, Ginhoux F, Newell EW. 2019. Dimensionality reduction for visualizing single-cell data using UMAP. *Nature Biotechnology* **37**:38–44. DOI: https://doi.org/10.1038/nbt.4314

Belgrader P, Cheng J, Maquat LE. 1993. Evidence to implicate translation by ribosomes in the mechanism by which nonsense codons reduce the nuclear level of human triosephosphate isomerase mRNA. *PNAS* **90**:482–486. DOI: https://doi.org/10.1073/pnas.90.2.482, PMID: 8421679

Boehm V, Haberman N, Ottens F, Ule J, Gehring NH. 2014. 3' UTR length and messenger ribonucleoprotein composition determine endocleavage efficiencies at termination codons. *Cell Reports* **9**:555–568. DOI: https://doi.org/10.1016/j.celrep.2014.09.012, PMID: 25310981

Bühler M, Steiner S, Mohn F, Paillusson A, Mühlemann O. 2006. EJC-independent degradation of nonsense immunoglobulin-mu mRNA depends on 3' UTR length. *Nature Structural & Molecular Biology* **13**:462–464. DOI: https://doi.org/10.1038/nsmb1081, PMID: 16622410

Butler A, Hoffman P, Smibert P, Papalexi E, Satija R. 2018. Integrating single-cell transcriptomic data across different conditions, technologies, and species. *Nature Biotechnology* **36**:411–420. DOI: https://doi.org/10.1038/nbt.4096, PMID: 29608179

Carter MS, Doskow J, Morris P, Li S, Nhim RP, Sandstedt S, Wilkinson MF. 1995. A regulatory mechanism that detects premature nonsense codons in T-cell receptor transcripts in vivo is reversed by protein synthesis inhibitors in vitro. *Journal of Biological Chemistry* **270**:28995–29003. DOI: https://doi.org/10.1074/jbc.270.48.28995, PMID: 7499432

Carter MS, Li S, Wilkinson MF. 1996. A splicing-dependent regulatory mechanism that detects translation signals. *The EMBO Journal* **15**:5965–5975. DOI: https://doi.org/10.1002/j.1460-2075.1996.tb00983.x, PMID: 8918474

Cau E, Gradwohl G, Fode C, Guillemot F. 1997. Mash1 activates a cascade of bHLH regulators in olfactory neuron progenitors. *Development* **124**:1611–1621. PMID: 9108377

Chan WK, Huang L, Gudikote JP, Chang YF, Imam JS, MacLean JA, Wilkinson MF. 2007. An alternative branch of the nonsense-mediated decay pathway. *The EMBO Journal* **26**:1820–1830. DOI: https://doi.org/10.1038/sj.emboj.7601628, PMID: 17363904

Chang YF, Imam JS, Wilkinson MF. 2007. The nonsense-mediated decay RNA surveillance pathway. *Annual Review of Biochemistry* **76**:51–74. DOI: https://doi.org/10.1146/annurev.biochem.76.050106.093909, PMID: 17352659

Chen M, Reed RR, Lane AP. 2019. Chronic inflammation directs an olfactory stem cell functional switch from neuroregeneration to immune defense. *Cell Stem Cell* **25**:501–513. DOI: https://doi.org/10.1016/j.stem.2019.08.011, PMID: 31523027

Chess A, Simon I, Cedar H, Axel R. 1994. Allelic inactivation regulates olfactory receptor gene expression. *Cell* **78**:823–834. DOI: https://doi.org/10.1016/S0092-8674(94)90562-2, PMID: 8087849

Clowney EJ, Magklara A, Colquitt BM, Pathak N, Lane RP, Lomvardas S. 2011. High-throughput mapping of the promoters of the mouse olfactory receptor genes reveals a new type of mammalian promoter and provides insight into olfactory receptor gene regulation. *Genome Research* **21**:1249–1259. DOI: https://doi.org/10.1101/gr.120162.110, PMID: 21705439

Colak D, Ji SJ, Porse BT, Jaffrey SR. 2013. Regulation of axon guidance by compartmentalized nonsense-mediated mRNA decay. *Cell* **153**:1252–1265. DOI: https://doi.org/10.1016/j.cell.2013.04.056, PMID: 23746841

Conti E, Izaurralde E. 2005. Nonsense-mediated mRNA decay: molecular insights and mechanistic variations across species. *Current Opinion in Cell Biology* **17**:316–325. DOI: https://doi.org/10.1016/j.ceb.2005.04.005, PMID: 15901503

Dalton RP, Lyons DB, Lomvardas S. 2013. Co-opting the unfolded protein response to elicit olfactory receptor feedback. *Cell* **155**:321–332. DOI: https://doi.org/10.1016/j.cell.2013.09.033, PMID: 24120133

Dooley JL, Abdel-Latif D, St Laurent CD, Puttagunta L, Befus D, Lacy P. 2009. Regulation of inflammation by Rac2 in immune complex-mediated acute lung injury. *American Journal of Physiology-Lung Cellular and Molecular Physiology* **297**:L1091–L1102. DOI: https://doi.org/10.1152/ajplung.90471.2008, PMID: 19801448

Dostie J, Dreyfuss G. 2002. Translation is required to remove Y14 from mRNAs in the cytoplasm. *Current Biology* **12**:1060–1067. DOI: https://doi.org/10.1016/S0960-9822(02)00902-8, PMID: 12121612

Doty RL. 2012. Olfactory dysfunction in parkinson disease. *Nature Reviews Neurology* **8**:329–339. DOI: https://doi.org/10.1038/nrneurol.2012.80, PMID: 22584158

Fletcher RB, Das D, Gadye L, Street KN, Baudhuin A, Wagner A, Cole MB, Flores Q, Choi YG, Yosef N, Purdom E, Dudoit S, Risso D, Ngai J. 2017. Deconstructing olfactory stem cell trajectories at Single-Cell resolution. *Cell Stem Cell* **20**:817–830. DOI: https://doi.org/10.1016/j.stem.2017.04.003, PMID: 28506465

Gajera CR, Emich H, Lioubinski O, Christ A, Beckervordersandforth-Bonk R, Yoshikawa K, Bachmann S, Christensen EI, Götz M, Kempermann G, Peterson AS, Willnow TE, Hammes A. 2010. LRP2 in ependymal cells regulates BMP signaling in the adult neurogenic niche. *Journal of Cell Science* **123**:1922–1930. DOI: https://doi.org/10.1242/jcs.065912, PMID: 20460439

Gallo RL, Kim KJ, Bernfield M, Kozak CA, Zanetti M, Merluzzi L, Gennaro R. 1997. Identification of CRAMP, a cathelin-related antimicrobial peptide expressed in the embryonic and adult mouse. *Journal of Biological Chemistry* **272**:13088–13093. DOI: https://doi.org/10.1074/jbc.272.20.13088, PMID: 9148921

Gehring NH, Kunz JB, Neu-Yilik G, Breit S, Viegas MH, Hentze MW, Kulozik AE. 2005. Exon-junction complex components specify distinct routes of nonsense-mediated mRNA decay with differential cofactor requirements. *Molecular Cell* **20**:65–75. DOI: https://doi.org/10.1016/j.molcel.2005.08.012, PMID: 16209946

Giorgi C, Yeo GW, Stone ME, Katz DB, Burge C, Turrigiano G, Moore MJ. 2007. The EJC factor eIF4AIII modulates synaptic strength and neuronal protein expression. *Cell* **130**:179–191. DOI: https://doi.org/10.1016/j.cell.2007.05.028, PMID: 17632064

Godfrey PA, Malnic B, Buck LB. 2004. The mouse olfactory receptor gene family. *PNAS* **101**:2156–2161. DOI: https://doi.org/10.1073/pnas.0308051100, PMID: 14769939

Gong Q. 2012. Culture of mouse olfactory sensory neurons. *Current Protocols in Neuroscience* **3**:24. DOI: https://doi.org/10.1002/0471142301.ns0324s58, PMID: 23042501

He F, Li X, Spatrick P, Casillo R, Dong S, Jacobson A. 2003. Genome-wide analysis of mRNAs regulated by the nonsense-mediated and 5′ to 3′ mRNA decay pathways in yeast. *Molecular Cell* **12**:1439–1452. DOI: https://doi.org/10.1016/S1097-2765(03)00446-5, PMID: 14690598

Hirota J, Mombaerts P. 2004. The LIM-homeodomain protein Lhx2 is required for complete development of mouse olfactory sensory neurons. *PNAS* **101**:8751–8755. DOI: https://doi.org/10.1073/pnas.0400940101, PMID: 15173589

Hongo T, Hakuba A, Shiota K, Naruse I. 2000. Suckling dysfunction caused by defects in the olfactory system in genetic arhinencephaly mice. *Neonatology* **78**:293–299. DOI: https://doi.org/10.1159/000014282, PMID: 11093009

Hornstein N, Torres D, Das Sharma S, Tang G, Canoll P, Sims PA. 2016. Ligation-free ribosome profiling of cell type-specific translation in the brain. *Genome Biology* **17**:149. DOI: https://doi.org/10.1186/s13059-016-1005-1, PMID: 27380875

Huang L, Lou CH, Chan W, Shum EY, Shao A, Stone E, Karam R, Song HW, Wilkinson MF. 2011. RNA homeostasis governed by cell type-specific and branched feedback loops acting on NMD. *Molecular Cell* **43**: 950–961. DOI: https://doi.org/10.1016/j.molcel.2011.06.031, PMID: 21925383

Huang L, Shum EY, Jones SH, Lou CH, Dumdie J, Kim H, Roberts AJ, Jolly LA, Espinoza JL, Skarbrevik DM, Phan MH, Cook-Andersen H, Swerdlow NR, Gecz J, Wilkinson MF. 2018. A Upf3b-mutant mouse model with behavioral and neurogenesis defects. *Molecular Psychiatry* **23**:1773–1786. DOI: https://doi.org/10.1038/mp.2017.173, PMID: 28948974

Hurt JA, Robertson AD, Burge CB. 2013. Global analyses of UPF1 binding and function reveal expanded scope of nonsense-mediated mRNA decay. *Genome Research* **23**:1636–1650. DOI: https://doi.org/10.1101/gr.157354.113, PMID: 23766421

Ibarra-Soria X, Levitin MO, Saraiva LR, Logan DW. 2014. The olfactory transcriptomes of mice. *PLOS Genetics* **10**:e1004593. DOI: https://doi.org/10.1371/journal.pgen.1004593, PMID: 25187969

Igarashi K, Kataoka K, Itoh K, Hayashi N, Nishizawa M, Yamamoto M. 1994. Regulation of transcription by dimerization of erythroid factor NF-E2 p45 with small maf proteins. *Nature* **367**:568–572. DOI: https://doi.org/10.1038/367568a0, PMID: 8107826

Iulianella A, Stanton-Turcotte D. 2019. The hedgehog receptor Patched1 regulates proliferation, neurogenesis, and axon guidance in the embryonic spinal cord. *Mechanisms of Development* **160**:103577. DOI: https://doi.org/10.1016/j.mod.2019.103577, PMID: 31634536

Iwema CL, Schwob JE. 2003. Odorant receptor expression as a function of neuronal maturity in the adult rodent olfactory system. *The Journal of Comparative Neurology* **459**:209–222. DOI: https://doi.org/10.1002/cne.10583, PMID: 12655505

Jaffrey SR, Wilkinson MF. 2018. Nonsense-mediated RNA decay in the brain: emerging modulator of neural development and disease. *Nature Reviews Neuroscience* **19**:715–728. DOI: https://doi.org/10.1038/s41583-018-0079-z, PMID: 30410025

Jarjour NN, Schwarzkopf EA, Bradstreet TR, Shchukina I, Lin CC, Huang SC, Lai CW, Cook ME, Taneja R, Stappenbeck TS, Randolph GJ, Artyomov MN, Urban JF, Edelson BT. 2019. Bhlhe40 mediates tissue-specific control of macrophage proliferation in homeostasis and type 2 immunity. *Nature Immunology* **20**:687–700. DOI: https://doi.org/10.1038/s41590-019-0382-5, PMID: 31061528

Johnson JL, Stoica L, Liu Y, Zhu PJ, Bhattacharya A, Buffington SA, Huq R, Eissa NT, Larsson O, Porse BT, Domingo D, Nawaz U, Carroll R, Jolly L, Scerri TS, Kim HG, Brignell A, Coleman MJ, Braden R, Kini U, et al. 2019. Inhibition of Upf2-Dependent Nonsense-Mediated decay leads to behavioral and neurophysiological abnormalities by activating the immune response. *Neuron* **104**:665–679. DOI: https://doi.org/10.1016/j.neuron.2019.08.027, PMID: 31585809

Jolly LA, Homan CC, Jacob R, Barry S, Gecz J. 2013. The UPF3B gene, implicated in intellectual disability, autism, ADHD and childhood onset schizophrenia regulates neural progenitor cell behaviour and neuronal outgrowth. *Human Molecular Genetics* **22**:4673–4687. DOI: https://doi.org/10.1093/hmg/ddt315, PMID: 23821644

Karam R, Lou CH, Kroeger H, Huang L, Lin JH, Wilkinson MF. 2015. The unfolded protein response is shaped by the NMD pathway. *EMBO Reports* **16**:599–609. DOI: https://doi.org/10.15252/embr.201439696, PMID: 25807986

Karousis ED, Mühlemann O. 2019. Nonsense-Mediated mRNA decay begins where translation ends. *Cold Spring Harbor Perspectives in Biology* **11**:a032862. DOI: https://doi.org/10.1101/cshperspect.a032862, PMID: 29891560

Kawauchi S, Kim J, Santos R, Wu HH, Lander AD, Calof AL. 2009. Foxg1 promotes olfactory neurogenesis by antagonizing Gdf11. *Development* **136**:1453–1464. DOI: https://doi.org/10.1242/dev.034967, PMID: 19297409

Kebaara BW, Atkin AL. 2009. Long 3'-UTRs target wild-type mRNAs for nonsense-mediated mRNA decay in *Saccharomyces cerevisiae*. *Nucleic Acids Research* **37**:2771–2778. DOI: https://doi.org/10.1093/nar/gkp146, PMID: 19270062

Kowalczyk MS, Tirosh I, Heckl D, Rao TN, Dixit A, Haas BJ, Schneider RK, Wagers AJ, Ebert BL, Regev A. 2015. Single-cell RNA-seq reveals changes in cell cycle and differentiation programs upon aging of hematopoietic stem cells. *Genome Research* **25**:1860–1872. DOI: https://doi.org/10.1101/gr.192237.115, PMID: 26430063

Kozak M. 1986. Point mutations define a sequence flanking the AUG initiator Codon that modulates translation by eukaryotic ribosomes. *Cell* **44**:283–292. DOI: https://doi.org/10.1016/0092-8674(86)90762-2, PMID: 3943125

Kurosaki T, Popp MW, Maquat LE. 2019. Quality and quantity control of gene expression by nonsense-mediated mRNA decay. *Nature Reviews Molecular Cell Biology* **20**:406–420. DOI: https://doi.org/10.1038/s41580-019-0126-2, PMID: 30992545

Lewcock JW, Reed RR. 2004. A feedback mechanism regulates monoallelic odorant receptor expression. *PNAS* **101**:1069–1074. DOI: https://doi.org/10.1073/pnas.0307986100, PMID: 14732684

Liao Y, Smyth GK, Shi W. 2014. featureCounts: an efficient general purpose program for assigning sequence reads to genomic features. *Bioinformatics* **30**:923–930. DOI: https://doi.org/10.1093/bioinformatics/btt656, PMID: 24227677

Logan DW, Brunet LJ, Webb WR, Cutforth T, Ngai J, Stowers L. 2012. Learned recognition of maternal signature odors mediates the first suckling episode in mice. *Current Biology* **22**:1998–2007. DOI: https://doi.org/10.1016/j.cub.2012.08.041, PMID: 23041191

Long AA, Mahapatra CT, Woodruff EA, Rohrbough J, Leung HT, Shino S, An L, Doerge RW, Metzstein MM, Pak WL, Broadie K. 2010. The nonsense-mediated decay pathway maintains synapse architecture and synaptic

vesicle cycle efficacy. *Journal of Cell Science* **123**:3303–3315. DOI: https://doi.org/10.1242/jcs.069468, PMID: 20826458

Love MI, Huber W, Anders S. 2014. Moderated estimation of fold change and dispersion for RNA-seq data with DESeq2. *Genome Biology* **15**:550. DOI: https://doi.org/10.1186/s13059-014-0550-8, PMID: 25516281

Lykke-Andersen S, Jensen TH. 2015. Nonsense-mediated mRNA decay: an intricate machinery that shapes transcriptomes. *Nature Reviews Molecular Cell Biology* **16**:665–677. DOI: https://doi.org/10.1038/nrm4063, PMID: 26397022

Lynch M, Marinov GK. 2015. The bioenergetic costs of a gene. *PNAS* **112**:15690–15695. DOI: https://doi.org/10.1073/pnas.1514974112, PMID: 26575626

Mabin JW, Woodward LA, Patton RD, Yi Z, Jia M, Wysocki VH, Bundschuh R, Singh G. 2018. The exon junction complex undergoes a compositional switch that alters mRNP structure and Nonsense-Mediated mRNA decay activity. *Cell Reports* **25**:2431–2446. DOI: https://doi.org/10.1016/j.celrep.2018.11.046, PMID: 30466796

Malnic B, Hirono J, Sato T, Buck LB. 1999. Combinatorial receptor codes for odors. *Cell* **96**:713–723. DOI: https://doi.org/10.1016/S0092-8674(00)80581-4, PMID: 10089886

Manglapus GL, Youngentob SL, Schwob JE. 2004. Expression patterns of basic helix-loop-helix transcription factors define subsets of olfactory progenitor cells. *The Journal of Comparative Neurology* **479**:216–233. DOI: https://doi.org/10.1002/cne.20316, PMID: 15452857

Mao H, Brown HE, Silver DL. 2017. Mouse models of Casc3 reveal developmental functions distinct from other components of the exon junction complex. *RNA* **23**:23–31. DOI: https://doi.org/10.1261/rna.058826.116, PMID: 27780844

Markenscoff-Papadimitriou E, Allen WE, Colquitt BM, Goh T, Murphy KK, Monahan K, Mosley CP, Ahituv N, Lomvardas S. 2014. Enhancer interaction networks as a means for singular olfactory receptor expression. *Cell* **159**:543–557. DOI: https://doi.org/10.1016/j.cell.2014.09.033, PMID: 25417106

McIntyre JC, Bose SC, Stromberg AJ, McClintock TS. 2008. Emx2 stimulates odorant receptor gene expression. *Chemical Senses* **33**:825–837. DOI: https://doi.org/10.1093/chemse/bjn061, PMID: 18854508

Mendell JT, Sharifi NA, Meyers JL, Martinez-Murillo F, Dietz HC. 2004. Nonsense surveillance regulates expression of diverse classes of mammalian transcripts and mutes genomic noise. *Nature Genetics* **36**:1073–1078. DOI: https://doi.org/10.1038/ng1429, PMID: 15448691

Michaloski JS, Galante PA, Malnic B. 2006. Identification of potential regulatory motifs in odorant receptor genes by analysis of promoter sequences. *Genome Research* **16**:1091–1098. DOI: https://doi.org/10.1101/gr.5185406, PMID: 16902085

Michel D, Moyse E, Brun G, Jourdan F. 1994. Induction of apoptosis in mouse [correction of rat] olfactory neuroepithelium by synaptic target ablation. *Neuroreport* **5**:1329–1332. PMID: 7919191

Miyamichi K, Serizawa S, Kimura HM, Sakano H. 2005. Continuous and overlapping expression domains of odorant receptor genes in the olfactory epithelium determine the dorsal/ventral positioning of glomeruli in the olfactory bulb. *Journal of Neuroscience* **25**:3586–3592. DOI: https://doi.org/10.1523/JNEUROSCI.0324-05.2005, PMID: 15814789

Nagy E, Maquat LE. 1998. A rule for termination-codon position within intron-containing genes: when nonsense affects RNA abundance. *Trends in Biochemical Sciences* **23**:198–199. DOI: https://doi.org/10.1016/S0968-0004(98)01208-0, PMID: 9644970

Nasif S, Contu L, Mühlemann O. 2018. Beyond quality control: the role of nonsense-mediated mRNA decay (NMD) in regulating gene expression. *Seminars in Cell & Developmental Biology* **75**:78–87. DOI: https://doi.org/10.1016/j.semcdb.2017.08.053, PMID: 28866327

Nguyen LS, Kim HG, Rosenfeld JA, Shen Y, Gusella JF, Lacassie Y, Layman LC, Shaffer LG, Gécz J. 2013. Contribution of copy number variants involving nonsense-mediated mRNA decay pathway genes to neuro-developmental disorders. *Human Molecular Genetics* **22**:1816–1825. DOI: https://doi.org/10.1093/hmg/ddt035, PMID: 23376982

Nguyen LS, Wilkinson MF, Gecz J. 2014. Nonsense-mediated mRNA decay: inter-individual variability and human disease. *Neuroscience & Biobehavioral Reviews* **46 Pt 2**:175–186. DOI: https://doi.org/10.1016/j.neubiorev.2013.10.016, PMID: 24239855

Notaras M, Allen M, Longo F, Volk N, Toth M, Li Jeon N, Colak D. 2019. UPF2 leads to degradation of dendritically targeted mRNAs to regulate synaptic plasticity and cognitive function. *Molecular Psychiatry* **21**:5. DOI: https://doi.org/10.1038/s41380-019-0547-5

Palacios IM. 2013. Nonsense-mediated mRNA decay: from mechanistic insights to impacts on human health. *Briefings in Functional Genomics* **12**:25–36. DOI: https://doi.org/10.1093/bfgp/els051, PMID: 23148322

Peterson J, Lin B, Barrios-Camacho CM, Herrick DB, Holbrook EH, Jang W, Coleman JH, Schwob JE. 2019. Activating a reserve neural stem cell population in Vitro Enables Engraftment and Multipotency after Transplantation. *Stem Cell Reports* **12**:680–695. DOI: https://doi.org/10.1016/j.stemcr.2019.02.014, PMID: 30930245

Qiu X, Mao Q, Tang Y, Wang L, Chawla R, Pliner HA, Trapnell C. 2017. Reversed graph embedding resolves complex single-cell trajectories. *Nature Methods* **14**:979–982. DOI: https://doi.org/10.1038/nmeth.4402, PMID: 28825705

Ramaiah M, Tan K, Plank TM, Song HW, Dumdie JN, Jones S, Shum EY, Sheridan SD, Peterson KJ, Gromoll J, Haggarty SJ, Cook-Andersen H, Wilkinson MF. 2019. A microRNA cluster in the Fragile-X region expressed during spermatogenesis targets FMR1. *EMBO Reports* **20**:e46566. DOI: https://doi.org/10.15252/embr.201846566, PMID: 30573526

Rebbapragada I, Lykke-Andersen J. 2009. Execution of nonsense-mediated mRNA decay: what defines a substrate? *Current Opinion in Cell Biology* **21**:394–402. DOI: https://doi.org/10.1016/j.ceb.2009.02.007, PMID: 19359157

Ressler KJ, Sullivan SL, Buck LB. 1994. A molecular dissection of spatial patterning in the olfactory system. *Current Opinion in Neurobiology* **4**:588–596. DOI: https://doi.org/10.1016/0959-4388(94)90061-2, PMID: 7812149

Riera CE, Tsaousidou E, Halloran J, Follett P, Hahn O, Pereira MMA, Ruud LE, Alber J, Tharp K, Anderson CM, Brönneke H, Hampel B, Filho CDM, Stahl A, Brüning JC, Dillin A. 2017. The sense of smell impacts metabolic health and obesity. *Cell Metabolism* **26**:198–211. DOI: https://doi.org/10.1016/j.cmet.2017.06.015, PMID: 28683287

Rodriguez S, Sickles HM, Deleonardis C, Alcaraz A, Gridley T, Lin DM. 2008. Notch2 is required for maintaining sustentacular cell function in the adult mouse main olfactory epithelium. *Developmental Biology* **314**:40–58. DOI: https://doi.org/10.1016/j.ydbio.2007.10.056, PMID: 18155189

Rozenkrantz L, Zachor D, Heller I, Plotkin A, Weissbrod A, Snitz K, Secundo L, Sobel N. 2015. A mechanistic link between olfaction and autism spectrum disorder. *Current Biology* **25**:1904–1910. DOI: https://doi.org/10.1016/j.cub.2015.05.048, PMID: 26144969

Salem S, Langlais D, Lefebvre F, Bourque G, Bigley V, Haniffa M, Casanova JL, Burk D, Berghuis A, Butler KM, Leahy TR, Hambleton S, Gros P. 2014. Functional characterization of the human dendritic cell immunodeficiency associated with the IRF8(K108E) mutation. *Blood* **124**:1894–1904. DOI: https://doi.org/10.1182/blood-2014-04-570879, PMID: 25122610

Sanz E, Yang L, Su T, Morris DR, McKnight GS, Amieux PS. 2009. Cell-type-specific isolation of ribosome-associated mRNA from complex tissues. *PNAS* **106**:13939–13944. DOI: https://doi.org/10.1073/pnas.0907143106, PMID: 19666516

Saraiva LR, Ibarra-Soria X, Khan M, Omura M, Scialdone A, Mombaerts P, Marioni JC, Logan DW. 2015. Hierarchical deconstruction of mouse olfactory sensory neurons: from whole mucosa to single-cell RNA-seq. *Scientific Reports* **5**:18178. DOI: https://doi.org/10.1038/srep18178, PMID: 26670777

Saraiva LR, Riveros-McKay F, Mezzavilla M, Abou-Moussa EH, Arayata CJ, Makhlouf M, Trimmer C, Ibarra-Soria X, Khan M, Van Gerven L, Jorissen M, Gibbs M, O'Flynn C, McGrane S, Mombaerts P, Marioni JC, Mainland JD, Logan DW. 2019. A transcriptomic atlas of mammalian olfactory mucosae reveals an evolutionary influence on food odor detection in humans. *Science Advances* **5**:eaax0396. DOI: https://doi.org/10.1126/sciadv.aax0396, PMID: 31392275

Schwob JE, Jang W, Holbrook EH, Lin B, Herrick DB, Peterson JN, Hewitt Coleman J. 2017. Stem and progenitor cells of the mammalian olfactory epithelium: taking poietic license. *Journal of Comparative Neurology* **525**:1034–1054. DOI: https://doi.org/10.1002/cne.24105, PMID: 27560601

Serizawa S, Miyamichi K, Nakatani H, Suzuki M, Saito M, Yoshihara Y, Sakano H. 2003. Negative feedback regulation ensures the one receptor-one olfactory neuron rule in mouse. *Science* **302**:2088–2094. DOI: https://doi.org/10.1126/science.1089122, PMID: 14593185

Serizawa S, Miyamichi K, Sakano H. 2004. One neuron-one receptor rule in the mouse olfactory system. *Trends in Genetics* **20**:648–653. DOI: https://doi.org/10.1016/j.tig.2004.09.006, PMID: 15522461

Serizawa S, Miyamichi K, Sakano H. 2005. Negative feedback regulation ensures the one neuron-one receptor rule in the mouse olfactory system. *Chemical Senses* **30**:i99–i100. DOI: https://doi.org/10.1093/chemse/bjh133, PMID: 15738216

Shang Y, Smith S, Hu X. 2016. Role of notch signaling in regulating innate immunity and inflammation in health and disease. *Protein & Cell* **7**:159–174. DOI: https://doi.org/10.1007/s13238-016-0250-0, PMID: 26936847

Shum EY, Jones SH, Shao A, Dumdie J, Krause MD, Chan WK, Lou CH, Espinoza JL, Song HW, Phan MH, Ramaiah M, Huang L, McCarrey JR, Peterson KJ, De Rooij DG, Cook-Andersen H, Wilkinson MF. 2016. The antagonistic gene paralogs Upf3a and Upf3b govern Nonsense-Mediated RNA decay. *Cell* **165**:382–395. DOI: https://doi.org/10.1016/j.cell.2016.02.046, PMID: 27040500

Sohni A, Tan K, Song HW, Burow D, de Rooij DG, Laurent L, Hsieh TC, Rabah R, Hammoud SS, Vicini E, Wilkinson MF. 2019. The neonatal and adult human testis defined at the Single-Cell level. *Cell Reports* **26**:1501–1517. DOI: https://doi.org/10.1016/j.celrep.2019.01.045, PMID: 30726734

Spies N, Burge CB, Bartel DP. 2013. 3' UTR-isoform choice has limited influence on the stability and translational efficiency of most mRNAs in mouse fibroblasts. *Genome Research* **23**:2078–2090. DOI: https://doi.org/10.1101/gr.156919.113, PMID: 24072873

Tan L, Li Q, Xie XS. 2015. Olfactory sensory neurons transiently express multiple olfactory receptors during development. *Molecular Systems Biology* **11**:844. DOI: https://doi.org/10.15252/msb.20156639, PMID: 26646940

Tan K, Wang Z, Zhang Z, An L, Tian J. 2016. IVF affects embryonic development in a sex-biased manner in mice. *Reproduction* **151**:443–453. DOI: https://doi.org/10.1530/REP-15-0588, PMID: 26825929

Tan K, Song HW, Wilkinson MF. 2020a. Single-cell RNAseq analysis of testicular germ and somatic cell development during the perinatal period. *Development* **147**:dev183251. DOI: https://doi.org/10.1242/dev.183251, PMID: 31964773

Tan K, Song HW, Thompson M, Munyoki S, Sukhwani M, Hsieh TC, Orwig KE, Wilkinson MF. 2020b. Transcriptome profiling reveals signaling conditions dictating human spermatogonia fate in vitro. *PNAS* **117**:17832–17841. DOI: https://doi.org/10.1073/pnas.2000362117, PMID: 32661178

Tarpey PS, Raymond FL, Nguyen LS, Rodriguez J, Hackett A, Vandeleur L, Smith R, Shoubridge C, Edkins S, Stevens C, O'Meara S, Tofts C, Barthorpe S, Buck G, Cole J, Halliday K, Hills K, Jones D, Mironenko T, Perry J,

et al. 2007. Mutations in UPF3B, a member of the nonsense-mediated mRNA decay complex, cause syndromic and nonsyndromic mental retardation. *Nature Genetics* **39**:1127–1133. DOI: https://doi.org/10.1038/ng2100, PMID: 17704778

Tepe B, Hill MC, Pekarek BT, Hunt PJ, Martin TJ, Martin JF, Arenkiel BR. 2018. Single-Cell RNA-Seq of mouse olfactory bulb reveals cellular heterogeneity and Activity-Dependent molecular census of Adult-Born neurons. *Cell Reports* **25**:2689–2703. DOI: https://doi.org/10.1016/j.celrep.2018.11.034, PMID: 30517858

Wachter A, Hartmann L. 2014. NMD: nonsense-mediated defense. *Cell Host & Microbe* **16**:273–275. DOI: https://doi.org/10.1016/j.chom.2014.08.015, PMID: 25211070

Wada M, Lokugamage KG, Nakagawa K, Narayanan K, Makino S. 2018. Interplay between coronavirus, a cytoplasmic RNA virus, and nonsense-mediated mRNA decay pathway. *PNAS* **115**:E10157–E10166. DOI: https://doi.org/10.1073/pnas.1811675115, PMID: 30297408

Wang SS, Tsai RY, Reed RR. 1997. The characterization of the Olf-1/EBF-like HLH transcription factor family: implications in olfactory gene regulation and neuronal development. *The Journal of Neuroscience* **17**:4149–4158. DOI: https://doi.org/10.1523/JNEUROSCI.17-11-04149.1997, PMID: 9151732

Whitman MC, Greer CA. 2009. Adult neurogenesis and the olfactory system. *Progress in Neurobiology* **89**:162–175. DOI: https://doi.org/10.1016/j.pneurobio.2009.07.003, PMID: 19615423

Woodward LA, Mabin JW, Gangras P, Singh G. 2017. The exon junction complex: a lifelong guardian of mRNA fate. *Wiley Interdisciplinary Reviews: RNA* **8**::e1411. DOI: https://doi.org/10.1002/wrna.1411

Zhang X, Firestein S. 2002. The olfactory receptor gene superfamily of the mouse. *Nature Neuroscience* **5**:124–133. DOI: https://doi.org/10.1038/nn800, PMID: 11802173

Zhang LJ, Gallo RL. 2016. Antimicrobial peptides. *Current Biology : CB* **26**:R14–R19. DOI: https://doi.org/10.1016/j.cub.2015.11.017, PMID: 26766224

Zheng S, Gray EE, Chawla G, Porse BT, O'Dell TJ, Black DL. 2012. PSD-95 is post-transcriptionally repressed during early neural development by PTBP1 and PTBP2. *Nature Neuroscience* **15**:381–388. DOI: https://doi.org/10.1038/nn.3026, PMID: 22246437

Zheng X, Boyer L, Jin M, Mertens J, Kim Y, Ma L, Ma L, Hamm M, Gage FH, Hunter T. 2016. Metabolic reprogramming during neuronal differentiation from aerobic glycolysis to neuronal oxidative phosphorylation. *eLife* **5**:e13374. DOI: https://doi.org/10.7554/eLife.13374, PMID: 27282387